◇ Monograph Excerpt ◇

Matter Antimatter Fluctuations

search, discovery and analysis of Bs flavor oscillations

Nuno Leonardo

Complete work published as:
Analysis of B_s oscillations at CDF, MIT Thesis (2006)
Matter antimatter fluctuations, Monograph, LAP Lambert (2011)

Chapter 5

Measurement of B mesons lifetimes

Having collected the data samples of B meson decays, their description in the mass and proper decay time spaces is achieved, and the B mesons lifetimes extracted.

5.1 Fitting technique

We develop a fitting framework based on the maximum likelihood estimation method, which we use to extract the parameters of interest from the B data samples. It is implemented in an *unbinned* fashion, where the input information provided directly to the fitter is that pertaining to the individual B meson candidates (these will be referred to as *events*). The unbinned likelihood description allows exploring more thoroughly the information contained in the data samples.

5.1.1 Maximum likelihood

The likelihood function $\mathcal{L}$ is a measure for the probability of observing the data set at hand, characterized by measurements $\mathbf{t} = \{t_i\}$, given the parameters $\boldsymbol{\tau} = \{\tau_j\}$. It is defined here as the joint probability density for the independent measurements $\mathbf{t}$ as a function of the parameters $\boldsymbol{\tau}$,

$$\mathcal{L}(\mathbf{t}|\boldsymbol{\tau}) = \prod_{\{t_i\}} \mathcal{P}(t_i|\boldsymbol{\tau})\,. \tag{5.1}$$

The model parameters $\boldsymbol{\tau}$ are varied, and their best estimates, denoted by *fitted* parameter values, correspond to the set which maximizes $\mathcal{L}$. This is implemented using the minimization program `Minuit` [72, 73], provided with the score function $-2\,\ln(\mathcal{L})$.

In case a fit to a common set of parameters is to be performed simultaneously to several B samples $\{s\}$, the product of the likelihoods $\mathcal{L}_s$ of individual samples is formed, and the

quantity to be minimized then becomes

$$-\,2\,\sum_{\{s\}}\,\ln\,\left(\mathcal{L}_s\right). \tag{5.2}$$

The necessary normalization of the underlying probability density function, $\int \mathcal{P} d\mathbf{t} = 1$, for each event, is implemented analytically, resulting in an optimization of the fitter speed and accuracy.

A given candidate has certain probabilities of belonging to the different components which form the sample being fit. The event likelihood is thus formed of terms describing these various components. In general, these contain the *signal* and *background* classes. Signal refers to those sample components the model description of which involve directly the parameters of interest. For the background components it is sufficient in general to provide an empirical description of the corresponding distributions. Denoting by f_B the fraction of background, and by $(1 - f_B)$ the fraction of signal, the likelihood becomes

$$\mathcal{L} = \prod_i \left[(1 - f_B) \cdot \mathcal{P}_i^S + f_B \cdot \mathcal{P}_i^B\right] \tag{5.3}$$

where $\mathcal{P}_i^S$ and $\mathcal{P}_i^B$ denote the signal and background likelihood components, evaluated for the i-th candidate.

More generally, the signal and background classes may be both formed of distinct components, which benefit from separate treatment in the likelihood model. The candidates forming such components may belong to one of the following categories:

- The nominal signal, where all tracks forming the candidate were correctly reconstructed as the B daughter particles of the decay channel being reconstructed.
- Partially reconstructed b-hadrons, where some tracks have not been reconstructed, or the decay products contain neutral particles.
- Misidentified tracks, where a particle has been wrongly reconstructed due to misidentification of a track with a lepton, pion, kaon, or proton.
- Misreconstructed B-decays, where, although the tracks have been assigned the correct masses, the resulting particles did not originate from the B decay being reconstructed.
- The combinatorial background, corresponding to other track combinations with an invariant mass lying in the mass fitting region.

The various specific components which contribute to each of the samples being fit have been identified in Section 4.3.

Each sample component is assigned corresponding PDFs in the spaces of the input variables. The likelihood is then formed of the joint PDFs, $\mathcal{P}^\alpha$, obtained for each component,

$$\mathcal{L} = \prod_i \sum_\alpha f_\alpha \mathcal{P}_i^\alpha \,, \tag{5.4}$$

where the indices i, α run over the number of events and number of sample components, respectively, and f_α denote the component fractions, with $\sum_\alpha f_\alpha = 1$.

While nominal signal and combinatorial background are in general the dominant contributions, in the following paragraphs we identify the specific realizations also of the other categories in our data samples.

5.1.2 Fit input variables

The quantities which serve as input to the fit include the mass, the proper decay time, and the proper decay time resolution of the reconstructed B candidates. These variables are introduced in the following, and will be denoted by the lower-case symbols m, t and σ_t, respectively.

Proper decay time

The principal measurements performed in this dissertation correspond to parameters which determine the distribution of the reconstructed proper decay time of B meson candidates. This quantity is related to the observed B candidate decay distance, and is defined as

$$t \equiv L_{xy} \frac{M^B}{p_T}. \tag{5.5}$$

Here p_T is the transverse momentum of the reconstructed system. L_{xy} is the projection on the direction of the transverse momentum p_T of the displacement vector in the transverse plane, $\vec{d}$, from the B meson production vertex to the its decay vertex,

$$L_{xy} = \vec{d} \cdot \frac{\vec{p}_T}{|p_T|}. \tag{5.6}$$

The world average value for the mass of the involved B meson, M^B, is used in the definition of t. For the signal PDF the fit estimate of the B mass is not used because it would introduce unnecessary uncertainties in the determination of t.

In case of fully reconstructed signal candidates, t is identified with the proper decay time of the B meson, $t = t^B$,

$$t^B = \frac{L^B}{\beta\gamma} = L^B \frac{M^B}{p^B} = L_{xy}^B \frac{M^B}{p_T^B}, \tag{5.7}$$

where L, β, and γ are the flight distance, velocity, and Lorentz boost factor of the B candidate.

For partially reconstructed decays, the B transverse momentum p_T^B, and thereby the B proper decay time t^B, cannot be measured. For example, the neutrino from the decay $B \to Dl\nu$ is not detected. In these cases t is sometimes also referred to as *pseudo*-proper decay time of the B candidate, and differs from t^B by a kinematic correction factor relating the B and Dl systems, $t^B = t \cdot \kappa$, defined by

$$\kappa = \frac{L_{xy}^B}{L_{xy}^{Dl}} \frac{p_T^{Dl}}{p_T^B}. \tag{5.8}$$

An average distribution, $\mathcal{F}(\kappa)$, for the κ-factor is obtained from Monte Carlo simulation, and this is a necessary ingredient when forming the signal PDF.

We will generally refer to the measured quantity t as proper decay time, while the prefix *pseudo* should be implicit for decays which are not completely reconstructed. Although t does not have a specific meaning for background components, it remains a well defined quantity, and is employed in both signal and background PDFs.

Proper decay time resolution

The detector resolution and track fitting methods imply a finite precision for the measurement of the B decay-length, $\sigma_{L_{xy}}$, and therefore in the determination of the proper decay time t,

$$\sigma_t = \sigma_{L_{xy}} \cdot \frac{M^B}{p_T}. \tag{5.9}$$

Contributions to the proper time resolution associated to uncertainties on the reconstructed transverse momentum and on the world average B masses are negligible. This information ought to be included in the relevant PDFs for the signal. Indeed, the proper decay time resolution is a determining factor in the B_s mixing analysis when attempting to resolve rapid, time dependent oscillations.

An additional complication arises from the fact that the uncertainty returned by the vertex fitter is in general underestimated, arising from the complexity of describing the track hit uncertainties. This requires a correcting *scale factor* to be applied,

$$\sigma_t \;\; \mapsto \;\; S_t \cdot \sigma_t \,. \tag{5.10}$$

This scale factor S_t is extracted directly from the data samples, as a fit parameter adjusting the Gaussian width describing a prompt component in the proper decay time distribution. However, such a prompt contribution is only present in $J/\psi K$ modes, and is suppressed by

the trigger selection in the other B samples. In those t biased samples of B^+ and B^0 decays a common average value for S_t is used. A more detailed study is performed in Section 5.7, in anticipation to the study of B_s oscillations, where the proper time uncertainty becomes a critical issue. In samples of B_s meson decays the scale factor S_t has an event dependent value, computed as described therein.

Mass

The inclusion of the reconstructed candidate mass, m, is crucial for separating signal from background components, and corresponding PDFs are included in the likelihood description.

In fully reconstructed decays it is the mass of the B candidate which is provided as input to the fit. For partially reconstructed decays, one uses instead the mass of the D meson candidate, as the B momentum is not completely reconstructed.

Although the B, or D, meson masses, M, will be parameters of the fit, the corresponding fit results for M should not be taken as definite measurements, the relevant systematic effects not being evaluated. We do not include the uncertainty on the candidate mass determination in the likelihood description.

5.1.3 Likelihood factors

The distributions of the fit input variables presented in the previous section – $m,\ t,\ \sigma_t$ – are described by likelihood factors, which for each sample component (e.g. signal, backgrounds) are given by

$$\mathcal{P} = L_m \, L_t \, L_{\sigma_t}. \tag{5.11}$$

The mass and proper time spaces are disjoint, and the corresponding probabilities multiply. The probability density for the proper time, t, depends on the smearing effect determined by the resolution σ_t. The factorization (5.11) is then

$$\mathcal{P}(m, t, \sigma_t) = \mathcal{P}(m) \cdot \mathcal{P}(t, \sigma_t) = \mathcal{P}(m) \cdot \mathcal{P}(t|\sigma_t) \cdot \mathcal{P}(\sigma_t). \tag{5.12}$$

These factors are the probability density functions of the corresponding argument variables, and are thus unit normalized

$$\int L_m \, dm = \int L_t \, dt = \int L_{\sigma_t} \, d\sigma_t = 1 \, .$$

The forms of the PDFs for mass and proper time, L_m and L_t, are given in the sections below in terms of the fitting parameters. The σ_t factor is obtained directly from data as follows: for the background, $L^B_{\sigma_t}$ is given by the σ_t distribution for events in the mass side-band region; for signal events, $L^S_{\sigma_t}$ corresponds to the normalized σ_t distribution obtained for

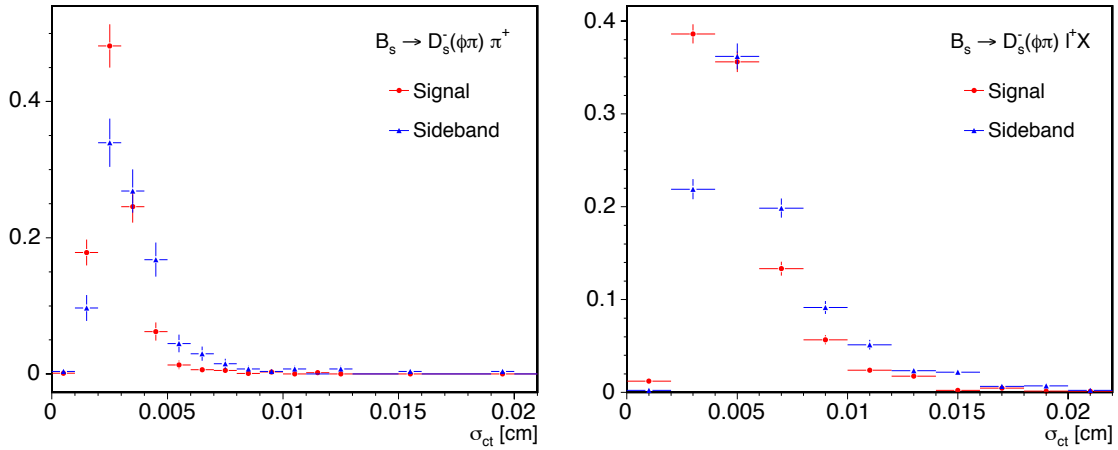

Figure 5.1: Distributions of calibrated proper decay time resolution σ_t, for signal and background events, for the main hadronic (left) and semileptonic (right) B_s decay modes.

candidates in the mass signal region, after mass side-band subtraction. These distributions are illustrated in Figure 5.1 for the indicated modes.

The components contributing to each sample are identified in Section 4.3 and summarized in Table 5.1. Separate likelihood terms as in (5.11) have to be provided for each component.

	signal	background
$J/\psi K$	B^+, B^0	combinatorial, Cabibbo-suppressed, K^* swap
$D\pi(\pi\pi)$	B^+, B^0, B_s	combinatorial, Cabibbo-suppressed, fully and partially rec.
Dl	B^+/B^0, B_s	combinatorial, physics, fakes

Table 5.1: Summary of data sample component categories, from Section 4.3.

5.2 Proper time likelihood formalism for signal

The proper decay time distribution for the signal is formed of an exponential decay characterized by the B meson lifetime τ, smeared by the detector resolution, and corrected by possible trigger, selection, and partial reconstruction effects.

5.2.1 Fully reconstructed and unbiased proper time

The expected true proper decay time follows an exponential decay form

$$E(t;\tau) = \frac{1}{\tau} e^{-\frac{t}{\tau}} \theta(t) = \begin{cases} 0, & t < 0 \\ \frac{1}{\tau} e^{-\frac{t}{\tau}}, & t \geq 0 \end{cases} \tag{5.13}$$

determined by the B meson lifetime, τ. The semicolon is used here to separate the main function argument from its parameters. The finite vertex resolution, described by a Gaussian function, induces the smearing of the expected proper time. The width of the resolution function is given by the measured proper time uncertainty for the individual event,

$$G(t;\sigma_t) = \frac{1}{\sqrt{2\pi}\sigma_t} e^{-\frac{t^2}{2\sigma_t^2}}. \tag{5.14}$$

The observable t is given by the sum of the true proper decay time (5.13) with the effect (jitter) of the detector resolution (5.14). The resulting PDF for t is accordingly given by the convolution of the two distributions,

$$\begin{aligned} L(t|\sigma_t,\tau) &= E(t;\tau) \otimes G(t;\sigma_t) \\ &= \int_{-\infty}^{\infty} \frac{1}{\tau} e^{-t'/\tau} \theta(t') \cdot \frac{1}{\sqrt{2\pi}\sigma_t} e^{-\frac{(t-t')^2}{2\sigma_t^2}} \, dt' \\ &= \frac{1}{2\tau} \, e^{-\frac{1}{\tau}(t-\frac{\sigma_t^2}{2\tau})} \cdot \mathrm{Erfc}\left(\frac{\sigma_t^2 - t\tau}{\sqrt{2}\sigma_t\tau}\right) \end{aligned} \tag{5.15}$$

The complementary error function, $\mathrm{Erfc}(z) \equiv \frac{2}{\sqrt{\pi}} \int_z^{\infty} e^{-u^2} du$, has been employed. That (5.15) has unit normalization follows from the fact that the normalization of the convolution of a function with a Gaussian coincides with the normalization of the function itself,

$$\int_{-\infty}^{+\infty} f(t) \otimes G(t) dt = \int_{-\infty}^{+\infty} f(t') \int_{-\infty}^{+\infty} G(t-t') dt \, dt' = \int_{-\infty}^{+\infty} f(t') dt' \,. \tag{5.16}$$

5.2.2 Fully reconstructed and biased proper time

Certain selection cuts, applied at either event triggering or reconstruction levels, may affect the expected proper time distribution, causing deviations from the shape given by (5.15).

For example, suppose a selection level threshold is applied directly to the proper time, $t > t_0$. Or, as it is most often the case, that such a cut is applied to the B meson decay-length or its significance, $L_{xy}/\sigma_{L_{xy}} > \alpha$. This translates again to applying a selection directly on the proper time, $t > t_\alpha$, where for each event the threshold is given by $t_\alpha = \alpha \cdot \left(\sigma_{L_{xy}} \frac{m_B}{p_T}\right)$. We note that such selection criteria are based on reconstructed, thus smeared, observables. The PDF becomes

$$L(t|\sigma_t,\tau,t_\alpha) = \frac{1}{\mathcal{N}} \cdot \frac{1}{2\tau} \, e^{-\frac{1}{\tau}(t-\frac{\sigma_t^2}{2\tau})} \cdot \mathrm{Erfc}\left(\frac{\sigma_t^2 - t\tau}{\sqrt{2}\sigma_t\tau}\right) \cdot \theta(t - t_\alpha) \,, \tag{5.17}$$

where the step function, $\theta(t)$, directly implements the selection $t > t_\alpha$. A normalization factor, $\mathcal{N}$, needs now to be evaluated, and this computation is to be performed for the individual events. For the case at hand, an analytical integration of (5.17) gives

$$\mathcal{N}(\sigma_t, \tau, t_\alpha) = \frac{1}{2}\left[e^{-\frac{1}{\tau}(t_\alpha - \frac{\sigma_t^2}{2\tau})} \cdot \mathrm{Erfc}\left(\frac{\sigma_t^2 - t_\alpha\tau}{\sqrt{2}\sigma_t\tau}\right) + \mathrm{Erfc}\left(\frac{t_\alpha}{\sqrt{2}\sigma_t}\right)\right] . \tag{5.18}$$

We have thus seen that in case a selection cut is imposed on an observable directly related to the proper decay time t, the effect on the PDF can be implemented through multiplication with an acceptance function, $\mathcal{E}(t)$, which in those cases is simply a step function, $\mathcal{E}(t) = \theta(t)$, centered at the corresponding cut value for each event. More generally, however, there are cuts which are not expressed as simple threshold conditions on t. The track impact parameter criterion is an example of such a cut. In these more complex cases, the sculpting effect on the proper time PDF can be described in a similar fashion,

$$\begin{aligned} L(t|\sigma_t, \tau) &= \frac{1}{\mathcal{N}} \cdot [\ E(t;\tau) \otimes G(t;\sigma_t)\ ] \cdot \mathcal{E}(t) \\ &= \frac{1}{\mathcal{N}} \cdot \frac{1}{2\tau}\ e^{-\frac{1}{\tau}(t - \frac{\sigma_t^2}{2\tau})} \cdot \mathrm{Erfc}\left(\frac{\sigma_t^2 - t\tau}{\sqrt{2}\sigma_t\tau}\right) \cdot \mathcal{E}(t) \end{aligned} \tag{5.19}$$

via an efficiency function, $\mathcal{E}(t)$. The normalization factor

$$\mathcal{N}(\sigma_t, \tau) = \int_{-\infty}^{\infty} \frac{1}{2\tau}\ e^{-\frac{1}{\tau}(t - \frac{\sigma_t^2}{2\tau})} \cdot \mathrm{Erfc}\left(\frac{\sigma_t^2 - t\tau}{\sqrt{2}\sigma_t\tau}\right) \cdot \mathcal{E}(t)\ dt \tag{5.20}$$

needs as before to be evaluated for each single event.

5.2.3 Partially reconstructed and biased proper time

For cases where the B meson is not fully reconstructed, the measured input observable t is related to the B meson proper decay time through a kinematical factor, obtained from Monte Carlo simulation. For semileptonic decays, such κ-factor has been defined in (5.8).

In this case, the original lifetime exponential of (5.13) takes the form

$$E'(t;\tau) = E(t;\tau) \otimes_\kappa \mathcal{F}(\kappa) = \int \frac{\kappa}{\tau} e^{-\frac{\kappa t}{\tau}} \theta(\kappa t) \cdot \mathcal{F}(\kappa)\ d\kappa \tag{5.21}$$

where $\mathcal{F}(\kappa)$ is the normalized κ-factor distribution, and the κ-factor smearing operator $\otimes_\kappa$ is defined by the second equality. In a similar fashion, the final PDF becomes

$$\begin{aligned} L(t|\sigma_t, \tau) &= \frac{1}{\mathcal{N}} \cdot [\ E(t;\tau) \otimes_\kappa \mathcal{F}(\kappa) \otimes G(t;\sigma_t)\ ] \cdot \mathcal{E}(t) \\ &= \frac{1}{\mathcal{N}} \cdot \int \frac{\kappa}{2\tau}\ \exp\left(-\frac{\kappa}{\tau}(t - \frac{\kappa\sigma_t^2}{2\tau})\right) \cdot \mathrm{Erfc}\left(\frac{\kappa\sigma_t^2 - t\tau}{\sqrt{2}\sigma_t\tau}\right) \cdot \mathcal{F}(\kappa)\ d\kappa \cdot \mathcal{E}(t)\,. \end{aligned} \tag{5.22}$$

The construction of the efficiency function, $\mathcal{E}(t)$, is specified in a later section, as is the evaluation of the normalization factor

$$\mathcal{N}(\sigma_t, \tau) \;=\; \int \left[\int_{-\infty}^{+\infty} e^{-\frac{\kappa}{\tau}t} \,\mathrm{Erfc}\left(\frac{\kappa\sigma_t^2 - t\tau}{\sqrt{2}\sigma_t\tau} \right) \,\mathcal{E}(t)\; dt \right] \cdot \frac{\kappa}{2\tau} \,\exp\left(\frac{\kappa^2\sigma_t^2}{2\tau^2} \right) \cdot \mathcal{F}(\kappa)\; d\kappa \,. \tag{5.23}$$

which needs to be performed for each event.

5.3 Describing trigger and reconstruction effects on proper time

The shape of the proper decay time distribution of a sample is potentially affected by trigger and reconstruction selection criteria. Such effects need to be incorporated into the relevant PDFs, along with the physics and resolution contributions. This is achieved by introducing an appropriate efficiency function, $\mathcal{E}(t)$, which multiplies the proper time signal PDF. Here we show how such functions are constructed, based on Monte Carlo simulation of the involved B decays, in which full detector effects, trigger, and offline selection are incorporated. The construction of the κ-factor distribution, necessary for partially reconstructed modes, is also presented.

5.3.1 The *t*-efficiency function

The t-efficiency function is defined as a function of the *reconstructed* proper decay time. This is appropriate as the selection criteria whose effect is to be described are themselves applied to reconstructed observables. An efficiency function defined in terms of un-smeared quantities is not compatible with a straightforward implementation of the t-resolution in the PDF [74].

The efficiency function $\mathcal{E}(t)$ relates the proper time distribution of a sample of events obtained with the given selection criteria, to the corresponding proper time distribution of the sample without the bias introduced by the selection. Indeed, it is constructed as the ratio of such two distributions. Specifically, the biased distribution is obtained directly from Monte Carlo simulation, where the description of the full biasing selection is included. And the denominator, describing the corresponding unbiased distribution, is obtained in an analytical fashion: the lifetime exponential smeared with the t-resolution, also obtained from the same Monte Carlo sample. That is, the t-efficiency function is given, for fully

reconstructed decays, by

$$\mathcal{E}(t) \;=\; \frac{t-\text{distribution after selection}}{\sum_{\{\sigma_t\}} \frac{1}{\tau} e^{-t/\tau} \otimes G(t;\sigma_t)}. \tag{5.24}$$

The parameter τ denotes the B^+, B^0 or B_s, as appropriate, lifetime value, identical to that used in the simulation from which the numerator is constructed [1]. The sum is weighted over the reconstructed proper time uncertainty distribution of the Monte Carlo simulated events. Figure 5.2 illustrates the t-efficiency distributions obtained for two selected hadronic modes.

For partially reconstructed decays a similar definition as in (5.24) is employed

$$\mathcal{E}(t) \;=\; \frac{t-\text{distribution after selection}}{\sum_{\{\sigma_t\}} \frac{1}{\tau} e^{-t/\tau} \otimes G(t;\sigma_t) \otimes_\kappa \mathcal{F}(\kappa)} \tag{5.25}$$

where the smearing with the κ-factor distribution $\mathcal{F}(\kappa)$ has been included in the construction of the unbiased distribution.

A t-efficiency function is constructed for each of the B mesons whose semileptonic decay channels contribute to a given sub-sample. This is done based on an inclusive Monte Carlo simulation containing all relevant channels. Figure 5.3 illustrates the t-efficiency distributions obtained for selected decay Dl sub-samples. These reflect the distinct pseudo proper time distributions which characterize the samples of B and D trigger types. For candidates for which the B-daughter lepton is not a trigger track (D trigger type) the t distribution is accordingly not suppressed as much by the trigger at low pseudo proper times.

We note that an overall scaling $\sigma_t \mapsto r \cdot \sigma_t$ is applied, in the definitions (5.24) and (5.25) above, to the reconstructed proper time uncertainties of the Monte Carlo events. The factor r is the Gaussian width of the distribution $(t^{\text{reconstructed}} - t^{\text{true}})/\sigma_t$, obtained from the Monte Carlo sample, and its numerical value is about 1.1.

5.3.2 The κ-factor distribution

The distribution $\mathcal{F}(\kappa)$ of κ-factors (5.8) is constructed for each B meson type present in each of the 24 Dl decay sub-samples from an inclusive Monte Carlo sample.

The κ-factor distribution is correlated to the mass of the Dl system, m_{Dl}. Indeed, the fraction of the B momentum which is reconstructed, quantified by the κ-factor, tends to be larger for candidates with larger m_{Dl}. That is, for candidates with m_{Dl} close to the B mass, not much momentum could have been carried away. Most importantly, such events tend to contribute a reduced spread for $\mathcal{F}(\kappa)$ as the phase space available for the missing neutrino, and additional non-reconstructed particles, is also reduced. This is shown explicitly

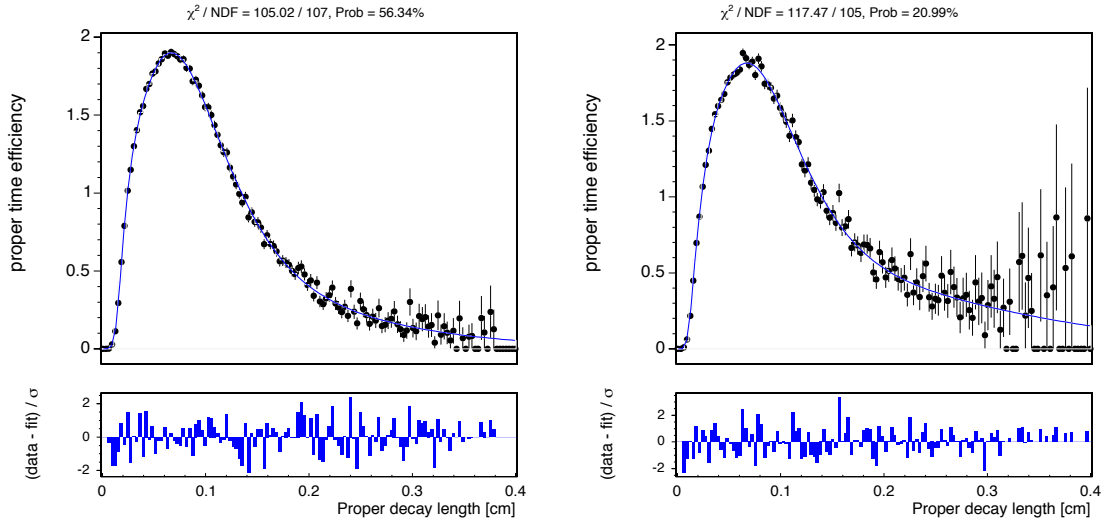

Figure 5.2: t-efficiency distribution and fitted function $\mathcal{E}(t)$for the fully reconstructed $B^+ \to \bar{D}^0\pi^+$ (left) and $B_s \to D_s^-[\phi\pi^-]\pi^+$ (right) decay channels

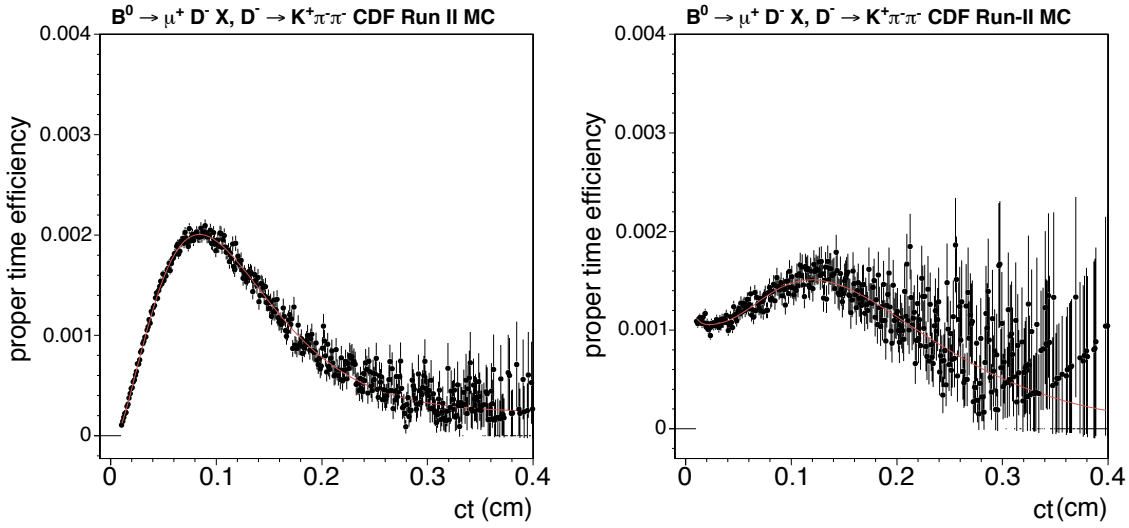

Figure 5.3: t-efficiency distribution and fitted function $\mathcal{E}(t)$for the partially reconstructed $B^0 \to D^-\mu^+X$ channels, for B trigger (left) and D trigger (right) type candidates.

in Figure 5.4. We exploit these dependences in the case of the D_sl samples, by assigning separate κ-factor distributions depending on the candidate's m_{D_sl}. Specifically the following

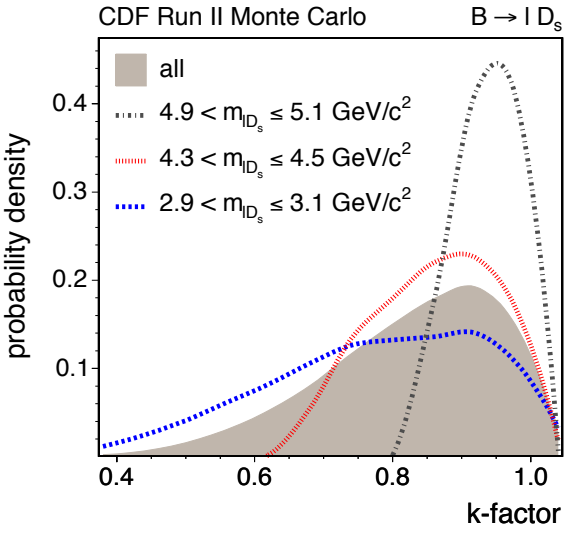

Figure 5.4: Distribution $\mathcal{F}(\kappa)$ of κ-factors, also shown for distinct ranges of the $D_s l$ mass.

ranges are used:

$$m_{D_s l} \in [1.0, 3.0],\ [3.0, 3.5],\ [3.5, 4.0],\ [4.0, 4.5],\ [4.5, 5.3]\ \mathrm{GeV/c^2}\ .$$

This classification is performed in view of the expected increased significance resulting from the better characterization of the κ-factor resolution of the candidates.

5.3.3 PDF normalization factor

We now address how the evaluation of the necessary PDF normalization factors, which have been defined in (5.20) and (5.23), is performed. We recall that these depend not only on fitting parameters, such as τ, but also on properties of the event, such as σ_t. Accordingly, the computation of these quantities needs to be performed at each iteration step of the fit, and for each event. The time required by the fit convergence process becomes a serious issue that needs to be addressed. We derive a convenient parameterization of the t-efficiency function which will allow us to perform an analytical integration in t of the PDFs in (5.19) and (5.22).

A given shape can in general be approximatively described by a number of templates. For example, in the rational approximation a shape is described by the ratio of two polynomials of certain degrees. Here however we are interested in finding simpler parameterizations, which will render the normalization integral feasible, by adding the least complexity to the remaining part of the PDF (to be multiplied by the t-efficiency itself). This reasoning leads to considering the class of functions represented by the basis $\{t^n e^{-t/\tau_n}\}$, resulting in a pa-

rameterization of the t-efficiency function involving terms of the following type

$$\mathcal{E}(t) \sim \sum_n \; a_n \; t^n \; e^{-\frac{t}{\tau_n}} \; \theta(t-\zeta_n). \tag{5.26}$$

We perform a fit to the t-efficiency curve defined for the t-biased modes, using a combination of templates of the form given in (5.26) up to second order, to determine the involved parameters $\{a_n, \tau_n, \zeta_n\}$. The following explicit forms are found convenient for the $D\pi(\pi\pi)$ and Dl modes, respectively:

$$\mathcal{E}(t) \;\; = \;\; \begin{cases} \sum_{j=0}^{2} a_j (t-\zeta_j)^2 e^{-\frac{t}{\tau_j}} \theta(t-\zeta_j) & \text{(hadronic)} \\ (a_0 + a_1\, t + a_2\, t^2) \left(f\, e^{-\frac{t}{\tau_1}} + (1-f)\, e^{-\frac{t}{\tau_2}} \right) \theta(t-\zeta) & \text{(semileptonic)} \end{cases} .$$

The fits to the t-efficiency curves are illustrated in Figure 5.2 for selected hadronic channels, and in Figure 5.3 for semileptonic modes where it can be seen that the latter expression accommodates well both B and D trigger type sub-samples.

The template expressions parameterizing the t-efficiency curves involve only terms of the form of (5.26). These then render the integrations in t expressed in (5.20) and (5.23) analytically feasible. The result of such calculations is explicitly included in Appendix .1. The additional integration involving the κ-factor distribution necessary for the semileptonic samples, both in the evaluation of the PDF (5.22) and its normalization (5.23), is performed numerically, by discretizing the $\mathcal{F}(\kappa)$ distribution and summing over the corresponding bins.

5.4 Mass PDF

The likelihood description of the mass subspace provides important separation power among the various signal and background components present in our samples.

For the nominal signal component, the width of the mass distribution is dominated by the detector resolution. The corresponding PDF will be given by a Gaussian function, unit-normalized in the fitting range $(M_{\min}, M_{\max})$,

$$G(m; M, \sigma_m, M_{\min}, M_{\max}) = \frac{\frac{1}{\sqrt{2\pi}\sigma_m} e^{-\frac{1}{2}\left(\frac{m-M}{\sigma_m}\right)^2}}{\frac{1}{2}\left[\mathrm{Erf}\left(\frac{M_{\max}-M}{\sqrt{2}\sigma_m} \right) + \mathrm{Erf}\left(\frac{M-M_{\min}}{\sqrt{2}\sigma_m} \right) \right]}, \tag{5.27}$$

with mean and width given by the fit parameters M and σ_m. The error function, $\mathrm{Erf}(z) \equiv \frac{2}{\sqrt{\pi}} \int_0^z e^{-u^2} du$, is used to express the normalization factor.

The combinatorial background is modeled through an empirical parameterization, as determined from the mass side-band region. For the $J/\psi K$ and Dl samples, a linear model

$am + b$ is employed. Upon unit-normalization in the mass fitting region $(M_{\rm min}, M_{\rm max})$, it is given by

$$A(m; a, M_{\rm min}, M_{\rm max}) \;=\; a\,m + \frac{1}{M_{\rm max} - M_{\rm min}} \left[1 - \frac{a}{2}\left(M^2_{\rm max} - M^2_{\rm min}\right)\right]. \qquad (5.28)$$

For the $D\pi$ modes an exponential shape is also found useful to model the combinatorial shape,

$$B(m; b, M_{\rm min}, M_{\rm max}) = \frac{be^{-bm}}{e^{-bM_{\rm min}} - e^{-bM_{\rm max}}}. \qquad (5.29)$$

In order to allow for a better determination of the background shape parameters, a preliminary fit is performed in an extended mass range.

$B^+ \to J/\psi K^+$

The nominal signal and combinatorial background are described by a Gaussian (5.27) and a linear (5.28) model, respectively,

$$\begin{aligned} L^{J/\psi K}_m(m|M, \sigma_m) &= G(m; M, \sigma_m, M_{\rm min}, M_{\rm max})\,, \\ L^{\rm comb}_m(m) &= A(m|a)\,. \end{aligned}$$

The contribution of the Cabibbo-suppressed $B^+ \to J/\psi\pi^+$ mode is fixed to 2.5% of the total B^+ signal, and its mass shape is taken from Monte Carlo simulation, being approximated by a Landau distribution. The template is positioned relative to the mass fit parameter, M, and is otherwise forced to those values found from simulation,

$$L^{J/\psi\pi}_m(m|M) \;=\; \frac{\left(m - M + \delta_{J/\psi\pi}\right)^6 e^{\frac{M-m-\delta_{J/\psi\pi}}{b}}}{a_6 b^7 - e^{\frac{M-M_{\rm max}-\delta_{J/\psi\pi}}{b}} \left[a_6 b^7 + \sum_{i=1}^{i=6} a_i b^i \left(M_{\rm max} - M + \delta_{J/\psi\pi}\right)^{7-i}\right]},$$

with $\vec{a} \equiv (1, 5, 30, 120, 360, 720)$, $\delta_{J/\psi\pi} = -3$ MeV/c^2, $b = 9$ MeV/c^2.

$B^0 \to J/\psi K^{*0}$

The description of the nominal signal and combinatorial background components is identical to that of the previous decay.

Candidates formed with an incorrect (*swapped*) mass assignment to the kaon-pion pair forming the K^* meson amount to a fraction of 16.9% relative to the nominal signal. The shape of its mass distribution is modeled by a Gaussian function centered at the nominal signal mass, as determined from Monte Carlo simulation,

$$L^{\rm swap}_m(m|M) \;=\; G(m; M, \sigma_{\rm swap}, M_{\rm min}, M_{\rm max}) \qquad \text{with} \quad \sigma_{\rm swap} = 25 \text{ MeV/c}^2\,.$$

$B^+ \to \bar{D}^0 \pi^+$

The mass distribution for the nominal signal is better described by a pair of Gaussian functions (5.27),

$$L_m^{D\pi}(m|M,\sigma_m) \;=\; (1-f)\,G(m;M,\sigma_m,M_{\rm min},M_{\rm max}) + f\,G(m;M,r\sigma_m,M_{\rm min},M_{\rm max})\,;$$

the factors f, r are found from a preliminary fit to the data performed in the wide mass range.

The combinatorial background is described by the combination of a linear (5.28) and an exponential (5.29) models,

$$L_m^{\rm comb}(m|b) \;=\; (1-f)\,A(m|a) \,+ f\,B(m;b,M_{\rm min},M_{\rm max})\,;$$

a flat $a = 0$ linear model is found to suffice. The relative fraction f of flat and exponential components as well as the exponential decay parameter b are determined from the wide mass range fit. Only the overall combinatorial background fraction is allowed to float in the narrow mass range fit.

The mass template for the misreconstructed Cabibbo-suppressed $B^+ \to \bar{D}^0 K^+$ mode is determined from Monte Carlo simulation. It is given by a Gaussian model whose width, relative fraction and displacement with respect to the nominal signal peak are fixed from simulation,

$$L_m^{DK}(m|M) \;=\; G(m;M-\delta_{DK},\sigma_{m_{DK}},M_{\rm min},M_{\rm max})\,,$$

with $\delta_{DK} = 57$ MeV/c^2 and $\sigma_{m_{DK}} = 27$ MeV/c^2.

$B^0 \to D^- \pi^+$

The nominal signal is described by a double-Gaussian model as the previous mode, and the combinatorial background by an exponential (5.29) model. A Gaussian model is used for the Cabibbo-suppressed $B^0 \to D^- K^+$ decay, identically to what was done for the previous decay mode.

The mass template $L_m^{B_s}(m)$ for the misreconstructed $B_s \to D_s^- \pi^+$ ($D_s^- \to K^+K^-\pi^-$) background is obtained from Monte Carlo simulation, and is given by two Gaussian functions centered at 5.315 GeV/c^2, of widths 45 MeV/c^2 and 22 MeV/c^2 with fractions 81% and 19%, respectively.

The misreconstructed $\Lambda_b^0 \to \Lambda_c^+ \pi^-$ ($\Lambda_c^+ \to p^+K^-\pi^+$) background decay is parameterized, $L_m^{\Lambda_b^0}(m)$, as well from Monte Carlo simulation by an exponential of decay constant 76 MeV/c^2 convoluted with a Gaussian of width 36 MeV/c^2 and centered at 5.439 GeV/c^2.

$B^+ \to \bar{D}^0\pi^+\pi^-\pi^+$, $B^0 \to D^-\pi^+\pi^-\pi^+$

The nominal signal and combinatorial background are described by single Gaussian (5.27) and falling exponential (5.29) models, respectively. The Cabibbo-suppressed $B \to DK\pi\pi$ decays are described by a Gaussian template whose width, displacement and fraction relative to the nominal signal are all determined, and fixed, from Monte Carlo simulation.

$B^0 \to D^{*-}\pi^+$

The mass of the nominal signal in $D^*\pi$ is modeled with a single Gaussian (5.27) component, while the Cabibbo-suppressed contribution from D^*K is handled by another Gaussian defined by parameters which are derived from signal Monte Carlo. The sole source of background events is combinatorics, which are well described in mass by a single linear (5.28) component.

$B^0 \to D^{*-}\pi^+\pi^-\pi^+$

The mass model is yet further simplified for the two modes with the $D^{*-}(\pi\pi\pi)^+$ topology as there is no Cabibbo-suppressed contribution to the B^0 signal. The mass subspace is entirely defined by a single Gaussian (5.27) peak on a linear (5.28) combinatorial background.

$B_s \to D_s^-\pi^+$, $B_s \to D_s^-\pi^+\pi^-\pi^+$

The nominal signals are described by a Gaussian function (5.27). The combinatorial background is modeled via the combination of a flat (5.28) and an exponential (5.29) distribution.

The Cabibbo-suppressed $B_s \to D_s^-K^+$ and $B_s \to D_s^-K^+\pi^-\pi^+$ decays are treated in an identical fashion to the previous modes, via a Gaussian model fixed from Monte Carlo. The shapes of the fully reconstructed Λ_b^0 and B^0 mass peaks are similarly fixed to those found from Monte Carlo. The same applies to the mass distributions from the partially reconstructed $B \to D_s^-\pi X$ background decays which are modeled with a Gaussian (5.27) and a linear (5.28) function.

$B^{+,0} \to Dl\,X$

To model the D mass distribution associated with the signals, and the *fakes* and *physics* background components we use a common double Gaussian distribution,

$$L_m^{Dl}(m|M,\sigma_{m,1},\sigma_{m,2}) = (1-f)\,G(m;M,\sigma_{m,1},M_{\min},M_{\max}) + f\,G(m;M,\sigma_{m,2},M_{\min},M_{\max})\,.$$

We assume a simple linear shape (5.28) for the mass distribution of the combinatorial background.

$\boldsymbol{B_s \to D_s^- l^+ X}$

The description in mass space of all involved components – signal as well as combinatorial, fakes, and physics backgrounds – is identical to that presented for the previous Dl samples.

5.5 Proper decay time PDF

The description of the proper decay time subspace involves the physics parameters which we are primarily interested in extracting from the data. The B mesons lifetimes do appear in the formalism developed in Section 5.2 for the signal components. The extraction of such parameters requires additionally an appropriate description of the other contributing components in the samples.

A background source common to all samples is that of the combinatorial type. Its description in the proper decay time space is found from the mass-sideband regions. A common *empirical* model is employed, which is found to provide an effective description across the data samples. It is first presented in a more general form, while its specific realizations for the individual samples are addressed afterwards. It involves a linear combination of Gaussian and smeared exponential terms. Terms of the latter form have been evaluated in (5.15). These are more generally written as

$$G_\alpha(t) \equiv G(t;\sigma_\alpha,\Delta_\alpha) = \delta(t-\Delta_\alpha)\otimes G(t;\sigma_\alpha)\,, \tag{5.30}$$

$$H_\alpha(t) \equiv H(t;\lambda_\alpha,\sigma_\alpha,\Delta_\alpha) = E(t-\Delta_\alpha;\lambda_\alpha)\otimes G(t;\sigma_\alpha)\,. \tag{5.31}$$

The model in its general form involves: one Gaussian term, one negatively and one positively short-lived exponential component, and one positively long-lived exponential component; let us refer to these by the subscripts $'o'$, $'-'$, $'+'$, $'++'$, respectively ($0 < \lambda_-, \lambda_+ \ll \lambda_{++}$). The resulting PDF may then be expressed as

$$\begin{aligned} &L_t^{\rm comb}(t|\sigma_o,\Delta_o,f_o;\lambda_-,\sigma_-,\Delta_-,f_-;\lambda_+,\sigma_+,\Delta_+,f_+;\lambda_{++},\sigma_{++},\Delta_{++},f_{++}) \\ &= \quad f_o G_o(t) + f_- H_-(-t) + f_+ H_+(t) + f_{++} H_{++}(t)\,, \end{aligned} \tag{5.32}$$

where $f_{\alpha\in\{o,-,+,++\}}$ denote the relative fractions, with $\sum_\alpha f_\alpha = 1$. Next we specify the model realizations (and simplifications) which are applied to the individual samples, and simultaneously attempt to motivate the above parameterization itself.

The description of the combinatorial background components in samples characterized by an *unbiased* proper decay time distribution is of special importance. The $J/\psi K$ modes provide such class of unbiased samples, for which the proper time distribution is dominated by a peak centered at $t = 0$. This is due to candidates constructed from tracks originating from

the primary vertex, which for the current case mostly involve the combination of a prompt J/ψ with prompt track(s). As the candidates forming this prompt component are characterized by zero proper time, its description is provided mathematically by a delta function, $\delta(t)$, convoluted with the resolution function (5.14); *i.e.* it is of the form of (5.30). The remaining sources of combinatorial background include: candidates involving tracks with erroneous hits, or belonging in reality to different displaced vertices (short-lived); physics backgrounds not explicitly accounted for, fake J/ψ from sequential semileptonic $b \to c\mu\nu \to s\mu\mu\nu\nu$ decays, or true displaced J/ψ paired with a random track (long-lived). The description of these other sources is provided, in an *effective* fashion, by the short and long-lived components of the form of (5.31). The combinatorial proper time PDF for the unbiased samples may be summarized as

$$\begin{aligned} & L_t^{\rm comb}(t|\sigma_t, S_t; \lambda_-, f_{++}; \lambda_+, f_+; \lambda_{++}, f_{++}) \\ = \quad & f_o G(t; S_t\sigma_t) + f_- H_-(-t) + f_+ H_+(t) + f_{++} H_{++}(t)\,. \end{aligned} \tag{5.33}$$

The displacement parameters are here taken to be zero, $\Delta_\alpha = 0$, and instead of the fitting parameters σ_α a common smearing resolution is used, which is determined for each event by the corresponding measured t-uncertainty, $\sigma_\alpha = S_t\sigma_t$. The scaling factor S_t is a fit parameter. As it was mentioned above, the prompt component formed of candidates with zero proper time should be described by the resolution function (5.14). In fact, deviations observed in the distribution of the data from this form must be due to an incorrect estimation of the t resolution, σ_t. The model of (5.33) thus allows the determination of the necessary proper time uncertainty scale factor from the fit to the data. Such correcting factor is propagated to the full likelihood model, and in particular to the signal proper time PDFs derived in Section 5.2.

For the biased samples, provided by the hadronic and semileptonic modes, the model of (5.32) is suitable with the following modifications. The trigger and candidate selection criteria remove events with lower proper times. This bias therefore substantially removes the negatively lived, H_-, and prompt, G_o, components. In effect, for the $D_{(s)}\pi(\pi\pi)$ modes a model without both such components is used, as it is found to describe data well. In the combinatorial PDF used for the $D_{(s)}l$ modes a Gaussian component displaced from the origin ($\Delta_o > 0$) is found useful to describe the data, and the negatively lived term is again not employed ($f_- = 0$).

We re-emphasize that the prompt component is substantially removed in the case of biased samples. This implies that the method for calibrating the proper time uncertainties which was described for the $J/\psi K$ modes cannot be applied to these samples in the same fashion. For the lifetime fits of the biased samples the t-uncertainties, which are inputs to the fit, are scaled with the predetermined factors S_t. This issue is addressed further

in Section 5.7, where we explain the details involved in determining and transferring these necessary correcting factors which are particularly relevant for the study of B_s oscillations performed in Chapter 8.

For the hadronic modes, the associated Cabibbo-suppressed channels share the same proper time description as the nominal signal components. Generally, associated exclusive backgrounds follow a model description provided by Monte Carlo simulation.

In the remainder of this section we describe the proper time PDFs of the additional background components which pertain to each individual sample.

$B^+ \to J/\psi K^+$

The proper decay time distribution for the nominal signal is that obtained in (5.15) for fully reconstructed, unbiased signal samples,

$$L(t|\sigma_t, S_t, \tau) \;=\; E(t;\tau) \otimes G(t; S_t\sigma_t)\,; \tag{5.34}$$

the scale factor S_t, as mentioned above, is introduced as a fit parameter. The Cabibbo-suppressed $B^+ \to J/\psi\pi^+$ component is described by a model identical to that of the signal, with a lifetime forced to $1.01\times\tau$ as predicted from simulation. The PDF for the combinatorial background is given in (5.33).

$B^0 \to J/\psi K^{*0}$

The model description of the nominal signal and combinatorial background is identical to that of the above charged mode. The proper time distribution of the K^*-swapped candidates is negligibly different from that of correctly reconstructed candidates, and share thus in the fit the same model as the nominal signal.

$B^+ \to \bar{D}^0\pi^+$

The proper time PDF for the nominal signal has been obtained in (5.19) for the fully reconstructed, biased samples. The Cabibbo-suppressed modes share the identical description. That for the combinatorial background is realized by two positively lived components of the form of (5.31), with a common displacement Δ_{bg} and smearing resolution parameter σ_{bg}.

$B^0 \to D^-\pi^+$

In addition to that referred to the previous mode, the Λ_b^0 and B_s^0 backgrounds are modeled from and fixed to Monte Carlo simulation via terms of the form of (5.31).

$B^+ \to \bar{D}^0\pi^+\pi^-\pi^+$, $B^0 \to D^-\pi^+\pi^-\pi^+$

The description employed for the nominal signal, as well as for the Cabibbo-suppressed modes, is that given in (5.19) for the fully reconstructed, biased samples. The combinatorial background, in the case of the $B^0 \to D^-\pi^+\pi^-\pi^+$ sample, is described by two independent, smeared exponential terms – of the form of (5.31) –, while for the $B^+ \to \bar{D}^0\pi^+\pi^-\pi^+$ sample one single such term is found adequate.

$B^0 \to D^{*-}\pi^+$

The nominal signal component in the t subspace is the standard expression derived for the hadronic modes (5.19), which is shared as well by the Cabibbo-suppressed D^*K component. The combinatorial background is fitted with two positively lived exponential tails. These tails share a common offset from zero, Δ_{bg}, and are smeared by a common Gaussian resolution whose width, σ_{bg}, is also a fit parameter.

$B^0 \to D^{*-}\pi^+\pi^-\pi^+$

The proper time distribution is modeled exactly as for $B^0 \to D^{*-}\pi^+$.

$B_s \to D_s^-\pi^+$, $B_s \to D_s^-\pi^+\pi^-\pi^+$

The proper time PDF for the nominal signal is that obtained in (5.19) for the fully reconstructed, biased samples. Such PDF is shared by the Cabibbo-suppressed modes. The same is also true for the partially reconstructed B_s candidates entering in the fit region. A more detailed analysis induces a κ-factor correction, analogous to that implemented for semileptonic modes, which for events in the considered mass range is very close to unit, and is thus neglected.

The shape of the combinatorial background is described by a single positively lived exponential component of the form of (5.31).

$B^{+,0} \to Dl\,X$

The reconstructed B signals in each of the three Dl samples involve both B^+ and B^0 meson decays. Accordingly, the proper decay time PDF must be formed of the combination

$$L_t^{Dl}(t|\sigma_t, \tau_u, \tau_d) \;=\; f_u \cdot L_t^u\,(t|\sigma_t, \tau_u) + f_d \cdot L_t^d\,(t|\sigma_t, \tau_d)\,. \tag{5.35}$$

Here τ_u and τ_d are the fit parameters, representing the B^+ and the B^0 meson lifetimes. The PDF components L^u and L^d are of the form of (5.22) as derived for the partially reconstructed,

biased samples. The involved t-efficiency functions and κ-factor distributions are derived independently for the combination of B^+ and of B^0 channels. The relative fractions f_u and f_d ($f_u + f_d = 1$) for the two components are computed from an inclusive Monte Carlo sample, assuming the world average values [1] for the sample composition parameters, a summary of which is provided in Table 4.16. The relative signal fraction f_d of B^0 mesons in the $D^0 l$, $D^+ l$ and $D^* l$ samples is about 29%, 86%, and 90%. The difference between the electron and muon samples is below 0.5%.

The combinatorial background is described by the general model expressed by (5.32) with absent negatively lived component ($f_- = 0$). A similar model is used for the *prompt* component, which is composed of one Gaussian (5.30) and one smeared exponential (5.31) term.

The physics backgrounds are described in an inclusive way by a Gaussian smeared exponential term of the form of (5.31).

$B_s \to D_s^- l^+ X$

The likelihood model for describing the t distribution of the nominal B_s signal component has been derived for the partially reconstructed modes and is expressed by (5.22).

Each physics background component is described by an independent t-PDF term of the form of that used for the signal. The corresponding PDF (5.22) is formed using a κ-factor distribution and a t-efficiency function which are derived from Monte Carlo simulation of the associated B signal decay. The nominal values of the B^+ and B^0 lifetimes [1] replace the B_s lifetime fit parameter when appropriate. The (pseudo) proper time t itself along with its uncertainty are determined, according to (5.5) and (5.9), using the nominal mass of the involved B meson.

5.6 Fitting procedure and results

In this section we present in further detail the procedure for performing the simultaneous mass and proper decay time fits to the data samples based on the models described previously, together with the extracted results.

The likelihood factors modeling the mass L_m and proper decay time L_t for the individual samples components have been presented in the Sections 5.4 and 5.5 above. Additionally, the proper decay time uncertainty likelihood factor L_{σ_t} is constructed. As discussed in Section 5.1.3, two such distributions are obtained for each mode, from the mass-sideband and signal (mass-sideband subtracted) regions, which are respectively associated to the combinatorial and to the remaining sample components.

Before fitting the data samples, the necessary Monte Carlo quantities and templates are computed and implemented in the fitting framework for each individual mode. These may involve t-efficiency functions (Section 5.3.1), κ-factor distributions (Section 5.3.2), and certain sample composition parameters and templates (Section 4.3).

In general, the fit to the data proceeds in several steps. The results of the fitted parameters obtained at each step are used to set the initial values, constrain or fix the parameter values for the following step. Combinatorial background parameters are inferred first. This is usually accomplished by fitting candidates which belong to the mass-sideband regions, in which case solely the combinatorial background model is employed. For the $D\pi(\pi\pi)$ samples, due to the structures that populate the lower mass-sideband region to the left of the signal peak, a preliminary fit is performed in an extended mass region, as in Section 4.3.2. In the Dl samples, information about further background sources is extracted from additional data samples, formed of selected fake candidates, as described in Section 4.3.3. In the final stages of the procedure, the fit is performed in the full signal region. The description of backgrounds may be relaxed as appropriate. The main parameters of interest, *i.e.* the B mesons lifetimes, are then finally extracted.

The correction to the proper time uncertainty is obtained directly from the fit in the case of the $J/\psi K$ decay modes. It corresponds to the parameter S_t introduced in (5.33). As mentioned before, these samples have a prominent prompt background component whose width readily allows for the determination of this parameter. That is not the case for the remaining samples, where such prompt components are highly suppressed by trigger and reconstruction requirements. For the B^+ and B^0 modes reconstructed in all $D\pi(\pi\pi)$ and Dl samples, a common correcting factor (5.10) is used. A value of 1.4 is employed, which is based on the results obtained from the mentioned $J/\psi K$ fit and according to average results also obtained in Section 5.7. While for the case of the B^+ and B^0 mesons the usage of a single numerical value is sufficient, for the B_s case a more detailed scale factor evaluation is necessary. For the B_s samples a scale factor is inferred for each candidate, according to the procedure explained in Section 5.7. The proper time uncertainties are thus scaled before being provided as input to the fit.

5.6.1 Fully reconstructed decays

All parameters of the fit model for the $J/\psi K$ modes are determined directly and at once from the fit to the data except for the amount and the shape of the Cabibbo-suppressed and K^{*0} swapped contributions. The fit results for these samples are shown in Table 5.4, and the fit projections are found in Figures 5.7 and 5.8.

In the case of the $D\pi(\pi\pi)$ modes, combinatorial background mass parameters are predetermined in a wide-range mass-only fit (Section 4.3.2). Among these only the overall combinatorial fraction is left floating in the nominal, narrow mass-range fit. The shape of the double-Gaussian model used in mass space to describe the signal peak in the $D\pi$ modes is also determined in such wide-range mass fit. No such preliminary fit is necessary in the case of the $D^*\pi(\pi\pi)$ modes for adjusting the simpler flat combinatorial mass model. The associated t-space parameters are then found from the fit to the candidates in the upper mass-sideband region. The relative fractions of the Cabibbo-suppressed and partially reconstructed decays are shown in Tables 4.10 and 4.9. These fractions along with the corresponding templates are determined from Monte Carlo simulation (Section 4.3). The fit projections are shown in Figures 5.9–5.21, and the numerical results are listed in Tables 5.5–5.8.

The B meson lifetimes as measured in the fully reconstructed modes are summarized in Table 5.2.

sample	$c\tau$ [μm]
$B^+ \to J/\psi K^+$	499.4±8.0
$B^+ \to \bar{D}^0\pi^+$	494.5±8.1
$B^+ \to \bar{D}^0\pi^\pm$	470.4±18.1
(combined B^+ fit	495.0±5.2)
$B^0 \to J/\psi K^{*0}$	458.4±11.0
$B^0 \to D^-\pi^+$	475.7±8.1
$B^0 \to D^-\pi^+\pi^-\pi^+$	458.4±11.5
$B^0 \to D^{*-}\pi^+$ ($\bar{D}^0 \to K^+\pi^-$)	495.3±22.4
$B^0 \to D^{*-}\pi^+$ ($\bar{D}^0 \to K^+\pi^-\pi^+\pi^-$)	449.7±19.6
$B^0 \to D^{*-}\pi^+\pi^-\pi^+$ ($\bar{D}^0 \to K^+\pi^-$)	449.3±21.0
$B^0 \to D^{*-}\pi^+\pi^-\pi^+$ ($\bar{D}^0 \to K^+\pi^-\pi^+\pi^-$)	489.5±24.0
(combined B^0 fit	468.1±4.8)
$B_s \to D_s^-\pi^+$, $D_s \to \phi\pi$	464.76±27.81
$B_s \to D_s^-\pi^+$, $D_s \to K^*K$	464.91±41.41
$B_s \to D_s^-\pi^+$, $D_s \to 3\pi$	417.89±58.15
$B_s \to D_s^-\pi^+\pi^-\pi^+$, $D_s \to \phi\pi$	590.38±89.30
$B_s \to D_s^-\pi^+\pi^-\pi^+$, $D_s \to K^*K$	514.07±106.39
(combined B_s fit	472.73±21.08)

Table 5.2: Summary of measured B lifetimes in fully reconstructed modes.

5.6.2 Partially reconstructed decays

For the semileptonic samples, the mass and the proper decay time models for the combinatorial background are adjusted by fitting candidates in the D mass-sideband regions. This is illustrated in Figure 5.5 for a selected sub-sample. The corresponding fraction is determined from the fit to the full signal mass region.

The relative fractions of the physics background are determined from Monte Carlo simulation and are summarized in Table 4.14 for all 24 semileptonic decay sub-samples. They are fixed parameters in the fit. Except in the case of the $D_s l$ samples, for which a signal-like treatment was adopted, a fixed, inclusive t template derived from Monte Carlo simulation is used to describe the proper decay time for the physics background component of each sub-sample. This is illustrated in Figure 5.5 for a selected sub-sample.

The description of the fakes background component is obtained from a preliminary fit to the fake lepton sample, as addressed in Section 4.3.3. This sample is sufficiently large to allow for the determination of the proper decay time distribution of the fakes background. Fit projections are shown in Figure 5.6. The relative fraction of this component is extracted from yet another preliminary fit, namely to the mass distribution of the Dl candidates, m_{Dl}. The procedure is thoroughly explained in Section 4.3.3. The numerical values of the fractions are summarized in Table 4.15. The characterization of the fakes background is fixed in the nominal lifetime fit. We note that the ability for background characterization carried by the Dl mass distributions, which was here used through a separate fit, could in principle be optimally exploited in a simultaneous fit. That is, by including m_{Dl} of the candidates as an additional input together with the corresponding likelihood factor.

For the $D^0 l$, $D^+ l$, $D^* l$ final states, all 12 decay sub-samples are fitted simultaneously. A different set of parameters is allocated for each of the sub-samples being fit, with the B^+ and the B^0 lifetimes as the only common parameters. The fit likelihood projections in the mass and pseudo proper decay time spaces are shown in Figures 5.22–5.33. The 12 decay $D_s l$ sub-samples are fitted individually. The fit projections are displayed in Figures 5.34–5.45.

The B meson lifetimes as measured in the partially reconstructed modes are summarized in Table 5.3.

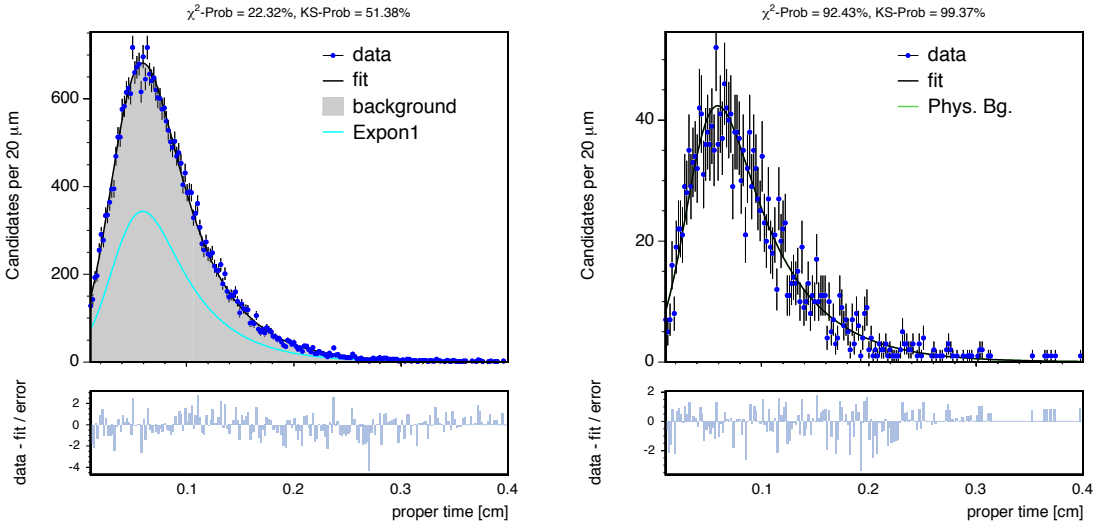

Figure 5.5: Proper decay time distribution of combinatorial (left) and physics (right) backgrounds, for the μD^+ B trigger sub-sample.

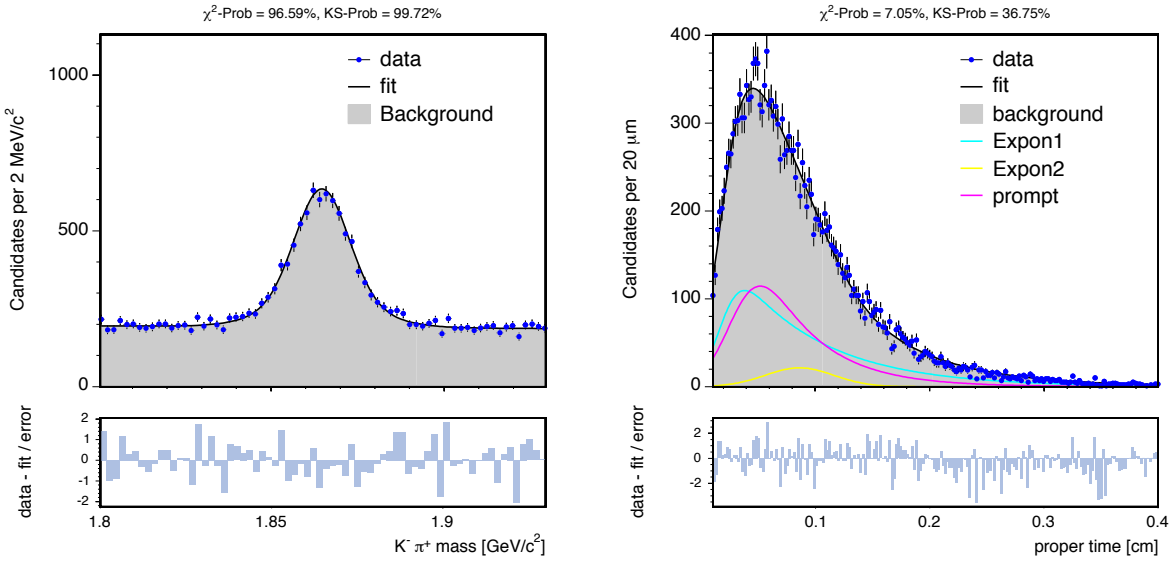

Figure 5.6: Fake lepton sample: mass and proper decay time distributions, for the μD^0 B trigger sub-sample.

Sub-sample	Trigger type	$c\tau_u$ [μm]	$c\tau_d$ [μm]	Sub-sample	Trigger type	$c\tau_s$ [μm]
μD^0	B	498.25±3.76	–	$\mu D_s(\phi\pi^-)$	B	440.8 ± 10.9
eD^0	B	489.55±4.66	–	$eD_s(\phi\pi^-)$	B	460.6 ± 14.7
μD^0	D	504.46±7.42	–	$\mu D_s(\phi\pi^-)$	D	471.2 ± 21.3
eD^0	D	502.63±9.62	–	$eD_s(\phi\pi^-)$	D	422.3 ± 25.8
μD^+	B	–	465.81± 4.36	$\mu D_s(K^{*0}K^-)$	B	437.9 ± 23.6
eD^+	B	–	462.82± 5.34	$eD_s(K^{*0}K^-)$	B	402.6 ± 27.9
μD^+	D	–	475.31± 7.38	$\mu D_s(K^{*0}K^-)$	D	445.6 ± 32.3
eD^+	D	–	460.31± 9.26	$eD_s(K^{*0}K^-)$	D	444.9 ± 45.7
μD^*	B	–	476.97± 7.25	$\mu D_s(\pi^+\pi^-\pi^-)$	B	392.2 ± 28.1
eD^*	B	–	468.35±10.41	$eD_s(\pi^+\pi^-\pi^-)$	B	409.4 ± 35.8
μD^*	D	–	459.31±12.62	$\mu D_s(\pi^+\pi^-\pi^-)$	D	480.0 ± 43.1
eD^*	D	–	448.24±16.41	$eD_s(\pi^+\pi^-\pi^-)$	D	420.6 ± 45.4
average		496.60±2.62	466.68± 2.53	average		441.14 ± 6.41

Table 5.3: Summary of measured B lifetimes in partially reconstructed modes; in the fits to the individual sub-samples the lifetime of a single B species is fitted, while those of the other present B mesons are fixed to their world average values [1].

parameter	$B^+ \to J/\psi K^+$	$B^0 \to J/\psi K^{*0}$
M[MeV/c^2]	5279.0 ± 0.2	5279.4 ± 0.3
σ [MeV/c^2]	12.8 ± 0.2	10.7 ± 0.3
f_{bg}	0.894 ± 0.002	0.863 ± 0.003
a	-1.09 ± 0.35	-1.78 ± 0.61
$c\tau$ [μm]	499.4 ± 8.0	458.4 ± 11.1
S_{ct}	1.334 ± 0.007	1.376 ± 0.013
f_+	0.061 ± 0.004	0.069 ± 0.007
f_{++}	0.021 ± 0.002	0.036 ± 0.006
f_-	0.012 ± 0.001	0.013 ± 0.002
$c\tau_+$ [μm]	79.0 ± 7.5	80.0 ± 12.6
$c\tau_{++}$ [μm]	448.5 ± 36.6	415.2 ± 40.7
$c\tau_-$ [μm]	138.4 ± 10.3	130.0 ± 16.0

Table 5.4: Mass and proper decay time fit results for $J/\psi K$ modes.

parameter	$B^+ \to \bar{D}^0\pi^+$	$B^0 \to D^-\pi^+$
M[MeV/c^2]	5278.3 ± 0.2	5278.6 ± 0.3
σ [MeV/c^2]	16.5 ± 0.2	16.2 ± 0.3
f_{bg}	0.390 ± 0.005	0.324 ± 0.007
$c\tau$ [μm]	494.5 ± 8.1	475.7 ± 8.1
f_{++}	0.800 ± 0.083	0.226 ± 0.613
$c\tau_+$ [μm]	477.2 ± 63.3	227.8 ± 39.8
$c\tau_{++}$ [μm]	208.5 ± 15.7	384.1 ± 149.6
Δ_{bg} [μm]	178.2 ± 3.0	205.9 ± 4.1
σ_{bg} [μm]	50.4 ± 2.1	55.5 ± 3.0

Table 5.5: Mass and proper decay time fit results for $D\pi$ modes.

parameter	$B^0 \to D^-\pi^+\pi^-\pi^+$	$B^+ \to \bar{D}^0\pi^+\pi^-\pi^+$
M[MeV/c^2]	5278.5 ± 0.4	5277.9 ± 0.5
σ [MeV/c^2]	14.2 ± 0.4	13.9 ± 0.5
f_{bg}	0.861 ± 0.004	0.527 ± 0.014
b [GeV/c^2]	1.330 ± 0.061	2.856 ± 0.261
$c\tau$ [μm]	458.4 ± 11.5	470.4 ± 18.1
$c\tau_+$ [μm]	436.2 ± 21.4	505.3 ± 15.2
Δ_+ [μm]	203.7 ± 7.8	268.5 ± 7.9
σ_+ [μm]	37.7 ± 4.3	75.2 ± 6.6
f_{++}	0.622 ± 0.089	—
$c\tau_{++}$ [μm]	281.8 ± 11.8	—
Δ_{++} [μm]	295.3 ± 9.3	—
σ_{++} [μm]	68.0 ± 3.1	—

Table 5.6: Mass and proper decay time fit results for $D\pi\pi\pi$ modes.

parameter		$D^0 \to K\pi$	$D^0 \to K\pi\pi\pi$
M	[MeV/c^2]	5278.1 ± 0.6	5279.3 ± 0.7
σ	[MeV/c^2]	18.2 ± 0.6	17.8 ± 0.6
f_{bg}		0.387 ± 0.016	0.299 ± 0.018
$slope$[GeV/c$^{2^{-1}}$]		-2.85 ± 0.96	-4.51 ± 1.33
$c\tau$	[μm]	495.3 ± 22.4	449.7 ± 19.6
f_{++}		0.047 ± 0.040	0.052 ± 0.051
$c\tau_+$	[μm]	221.9 ± 17.5	241.2 ± 25.7
$c\tau_{++}$	[μm]	970.6 ± 386.0	1104.1 ± 509.9
Δ_{bg}	[μm]	100.3 ± 4.3	81.1 ± 5.3
σ_{bg}	[μm]	24.7 ± 3.5	22.2 ± 4.3

Table 5.7: Mass and proper decay time fit results for $B^0 \to D^{*-}\pi^+$ modes, fitted separately by D^0 decay channel.

parameter		$D^0 \to K\pi$	$D^0 \to K\pi\pi\pi$
M	[MeV/c^2]	5277.9 ± 0.7	5277.4 ± 0.7
σ	[MeV/c^2]	15.5 ± 0.7	14.6 ± 0.7
f_{bg}		0.726 ± 0.011	0.676 ± 0.014
$slope$[GeV/c$^{2^{-1}}$]		-3.29 ± 0.44	-3.36 ± 0.56
$c\tau$	[μm]	449.3 ± 21.0	489.5 ± 24.0
f_{++}		0.088 ± 0.073	0.468 ± 0.274
$c\tau_+$	[μm]	206.3 ± 13.5	181.5 ± 46.5
$c\tau_{++}$	[μm]	496.3 ± 134.8	359.1 ± 63.8
Δ_{bg}	[μm]	152.0 ± 2.9	141.3 ± 3.7
σ_{bg}	[μm]	37.3 ± 2.3	29.9 ± 2.8

Table 5.8: Mass and proper decay time fit results for $B^0 \to D^{*-}(\pi\pi\pi)^+$ modes, fitted separately by D^0 decay channel.

parameter		$B_s \to D_s^- \pi^+$ channels		
		$D_s^- \to \phi\pi^-$	$D_s^- \to K^{*0}K^-$	$D_s^- \to \pi^-\pi^+\pi^-$
m	[GeV/c^2]	5.365272 ± 0.001206	5.369043 ± 0.001358	5.367352 ± 0.000037
σ	[GeV/c^2]	0.021013 ± 0.001195	0.016042 ± 0.001234	0.021484 ± 0.002567
f_{bg}		0.436024 ± 0.019620	0.517976 ± 0.029545	0.728162 ± 0.029775
τ_{bg}	[GeV/c^2]	0.436343 ± 0.118268	2.439732 ± 0.183415	1.468729 ± 0.145326
f_{bg}^{lin}	[GeV/c^2]	—	0.498256 ± 0.163246	—
$c\tau$	[cm]	0.046476 ± 0.002781	0.046491 ± 0.004141	0.041789 ± 0.005815
backgr. $c\tau$	[cm]	0.019139 ± 0.001303	0.022452 ± 0.001757	0.019421 ± 0.001425
backgr. offset	[cm]	0.012299 ± 0.000738	0.014345 ± 0.000837	0.019063 ± 0.000819
backgr. σ	[cm]	0.003431 ± 0.000644	0.003639 ± 0.000706	0.004524 ± 0.000664

Table 5.9: Mass and proper decay time fit results for $B_s \to D_s^- \pi^+$ modes.

parameter		$B_s \to D_s^- \pi^+ \pi^- \pi^+$ channels	
		$D_s^- \to \phi\pi^-$	$D_s^- \to K^{*0}K^-$
m	[GeV/c^2]	5.368652 ± 0.000002	5.368372 ± 0.001627
σ	[GeV/c^2]	0.013856 ± 0.001497	—
f_{bg}		0.844878 ± 0.015780	0.857557 ± 0.026283
τ_{bg}	[GeV/c^2]	1.138907 ± 0.085058	1.359105 ± 0.124292
$c\tau$	[cm]	0.059038 ± 0.008930	0.049950 ± 0.002930
backgr. $c\tau$	[cm]	0.046073 ± 0.001930	0.051407 ± 0.010639
backgr. offset	[cm]	0.026917 ± 0.001065	0.033521 ± 0.001842
backgr. σ	[cm]	0.007232 ± 0.000944	0.010109 ± 0.001550

Table 5.10: Mass and proper decay time fit results for $B_s \to D_s^- \pi^+ \pi^- \pi^+$ modes.

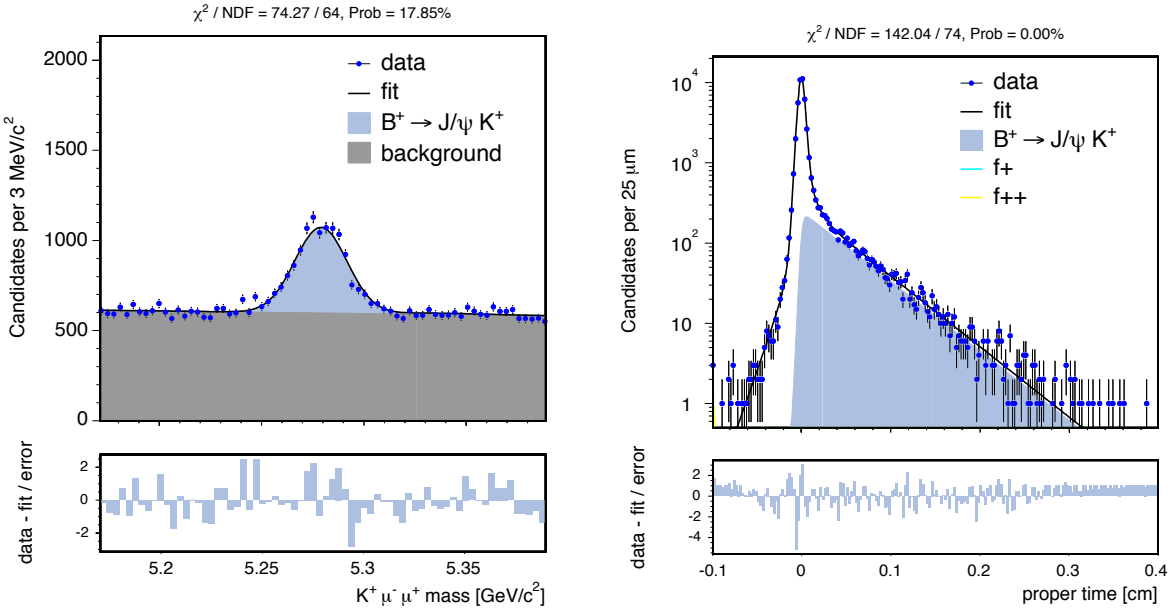

Figure 5.7: Mass and proper decay time fit projections for $B^+ \to J/\psi K^+$ decay.

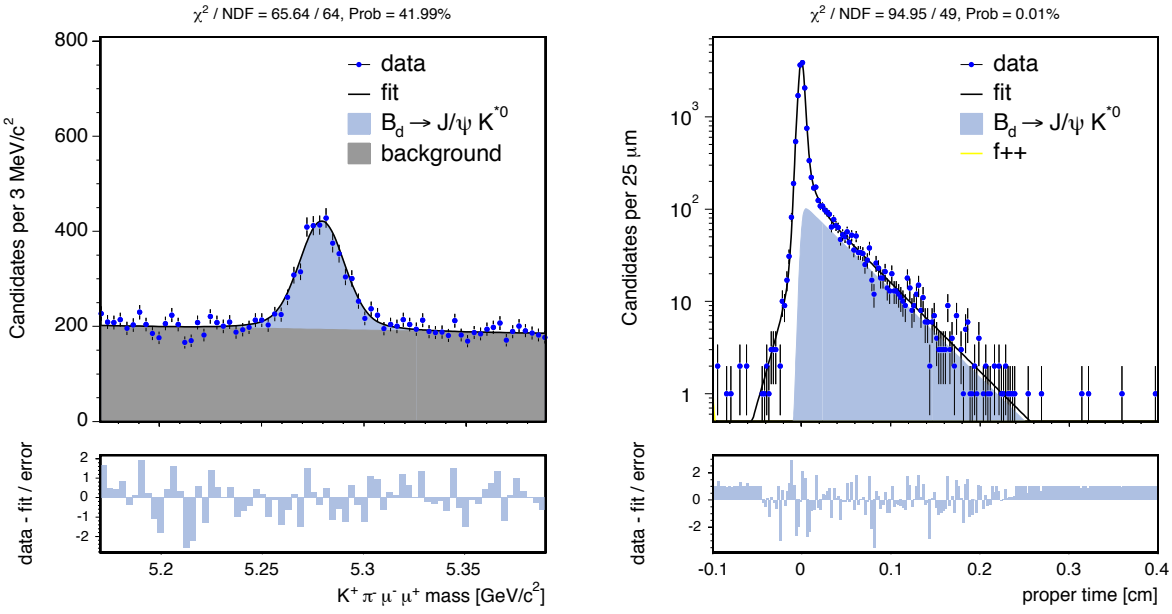

Figure 5.8: Mass and proper decay time fit projections for $B^0 \to J/\psi K^{*0}$ decay.

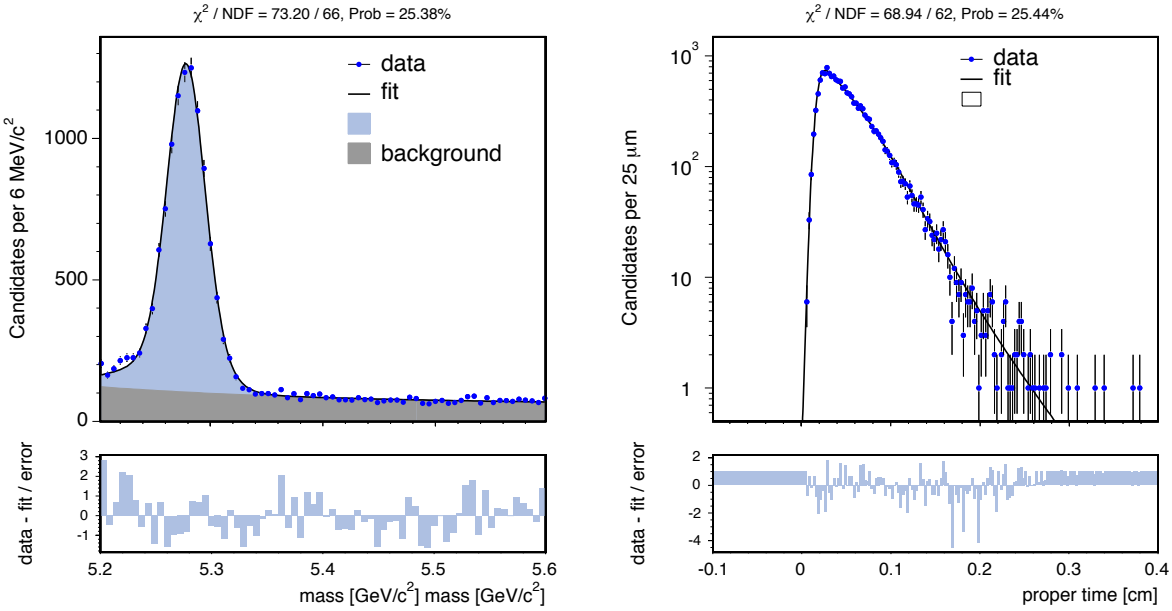

Figure 5.9: Mass and proper decay time fit projections for $B^+ \to \bar{D}^0\pi^+$ decay.

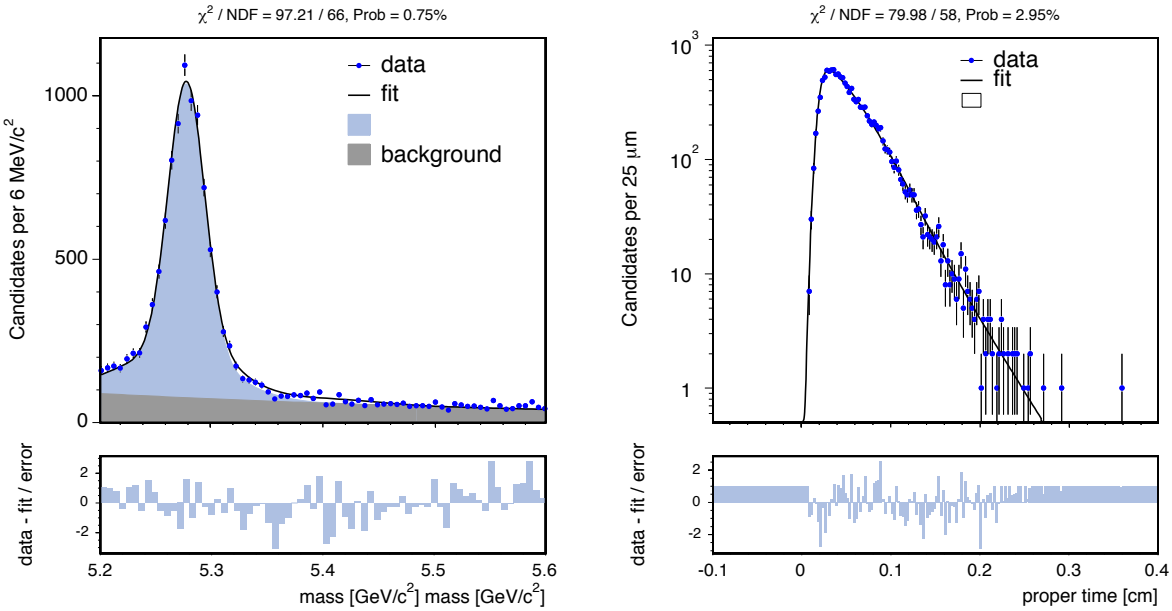

Figure 5.10: Mass and proper decay time fit projections for $B^0 \to D^-\pi^+$ decay.

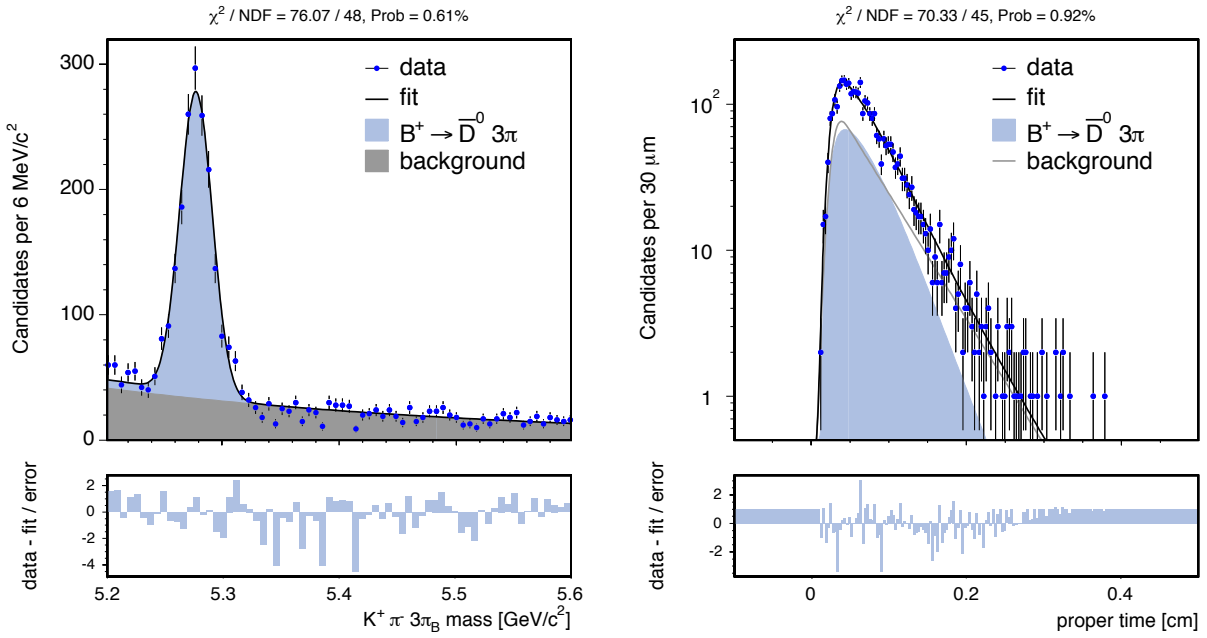

Figure 5.11: Mass and proper decay time fit projections for the $B^+ \to \bar{D}^0\pi^+\pi^-\pi^+$ decay.

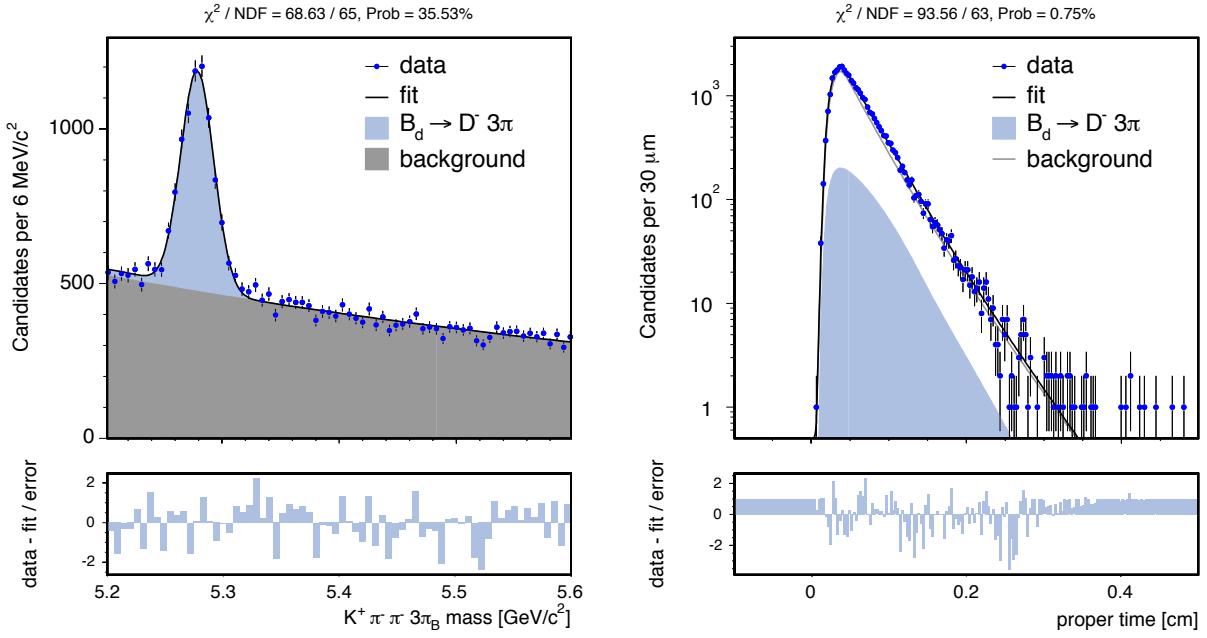

Figure 5.12: Mass and proper decay time fit projections for the $B^0 \to D^-\pi^+\pi^-\pi^+$ decay.

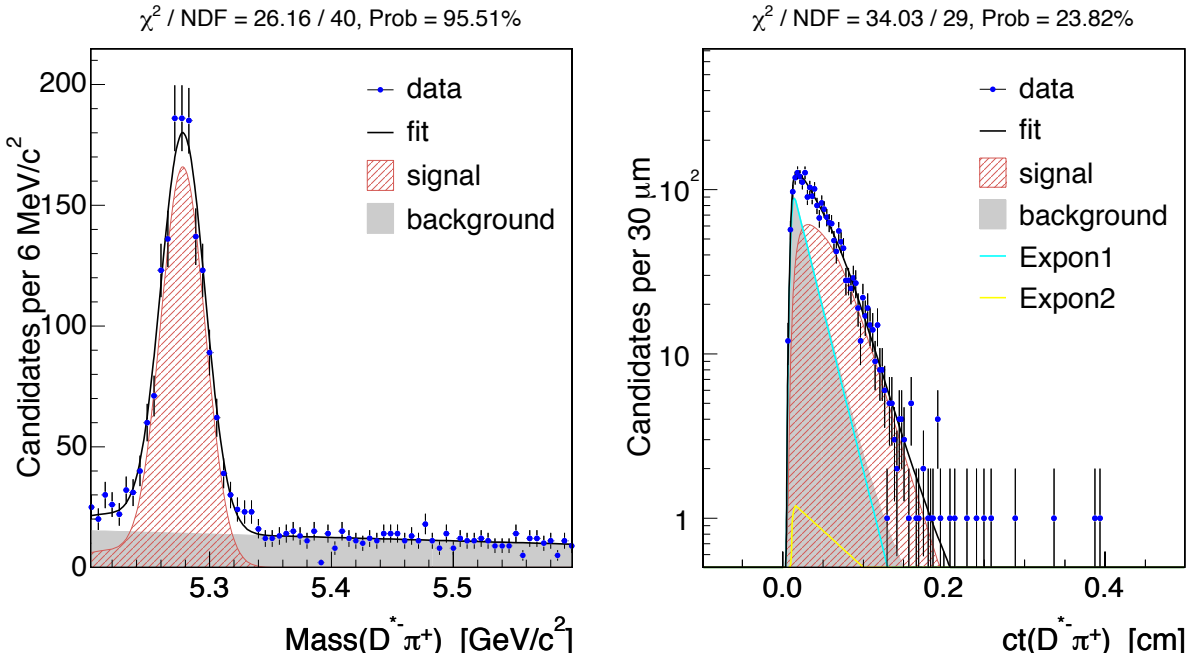

Figure 5.13: Mass and proper decay time fit projections for $B^0 \to D^{*-}\pi^+$, with $D^0 \to K\pi$.

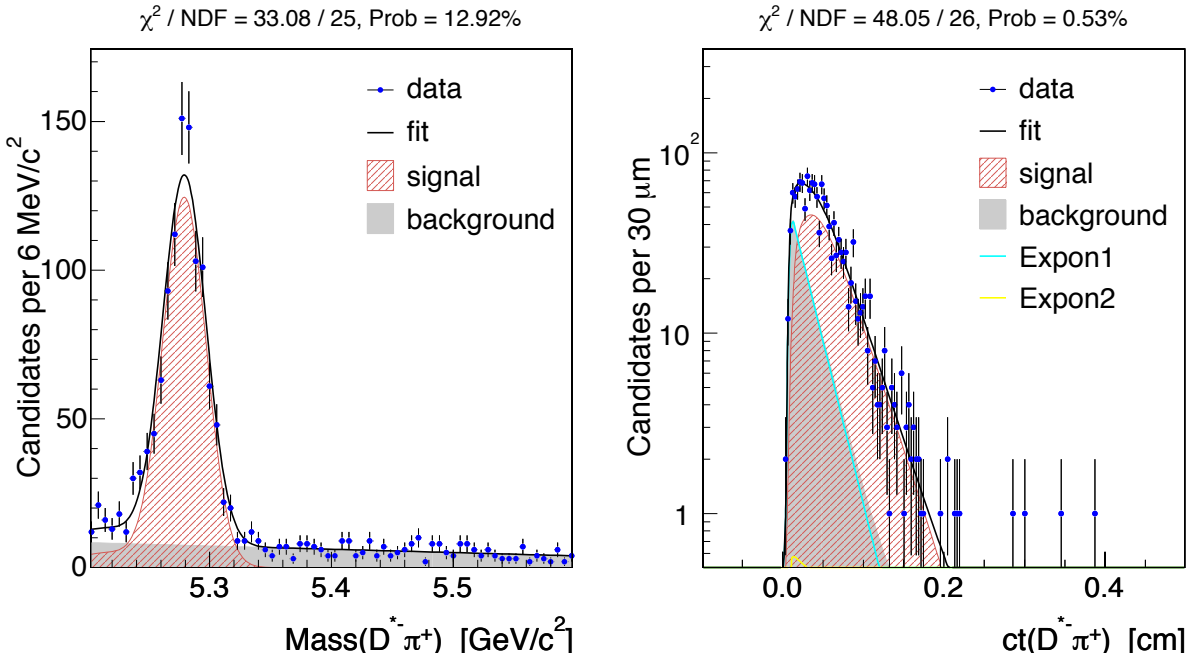

Figure 5.14: Mass and proper decay time fit projections for $B^0 \to D^{*-}\pi^+$, with $D^0 \to K\pi\pi\pi$.

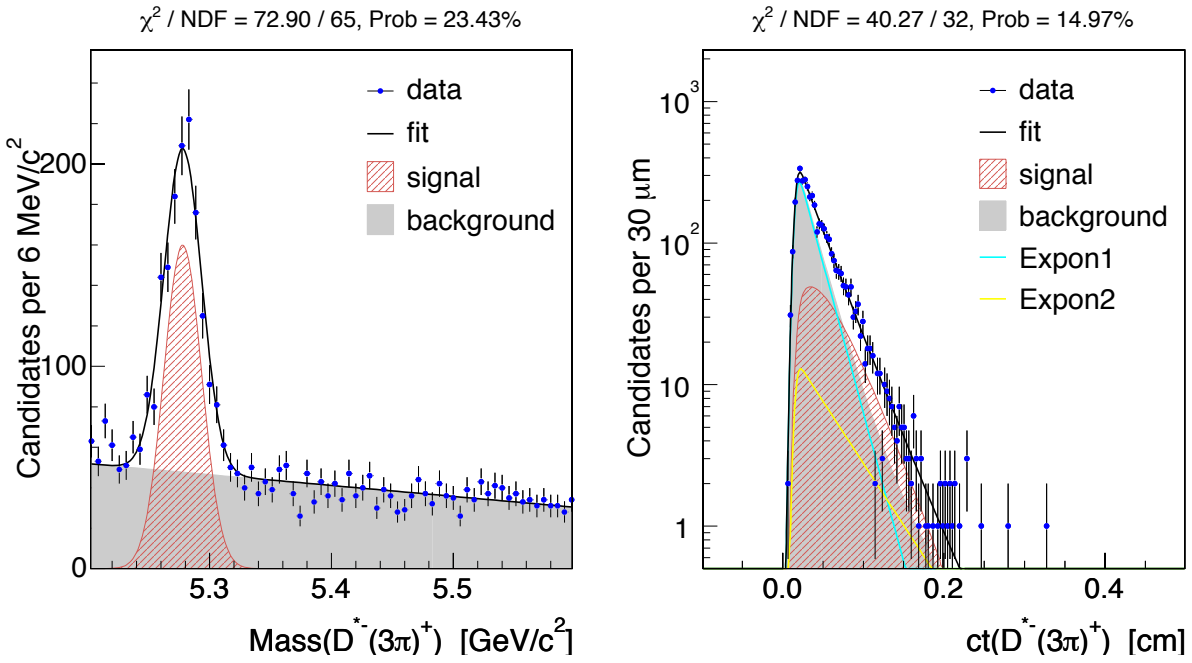

Figure 5.15: Mass and proper decay time fit projections for $B^0 \to D^{*-}(\pi\pi\pi)^+$, with $D^0 \to K\pi$.

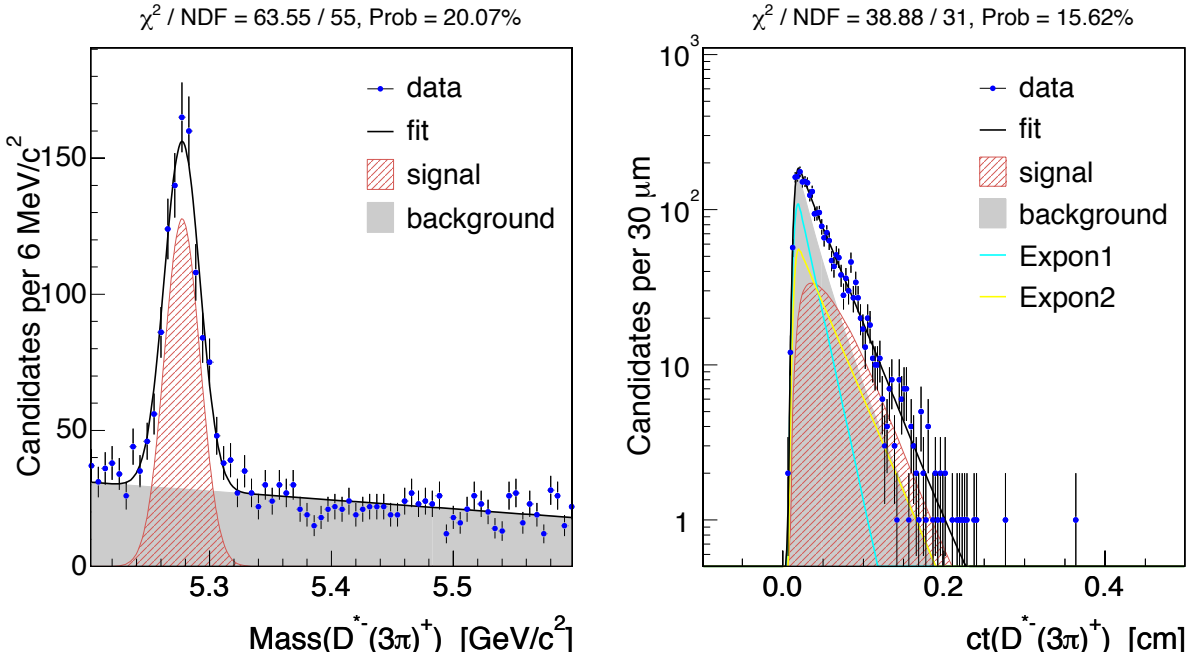

Figure 5.16: Mass and proper decay time fit projections for $B^0 \to D^{*-}(\pi\pi\pi)^+$, with $D^0 \to K\pi\pi\pi$.

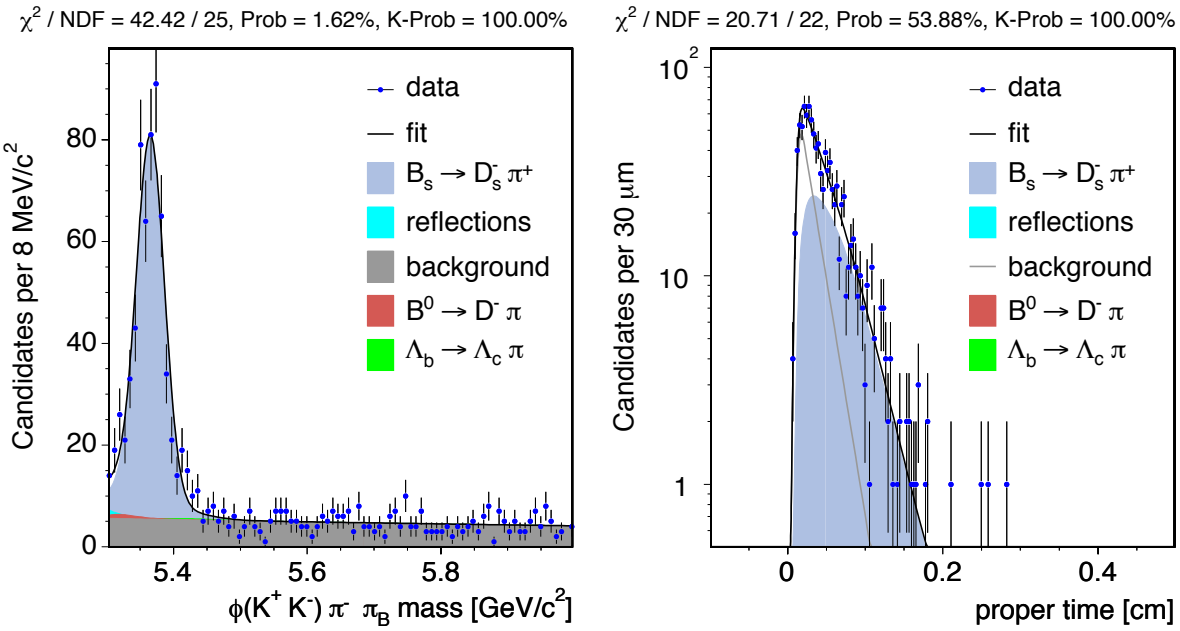

Figure 5.17: Mass and proper decay time fit projections for $B_s \to D_s^- \pi^+$ with $D_s^- \to \phi\pi^-$.

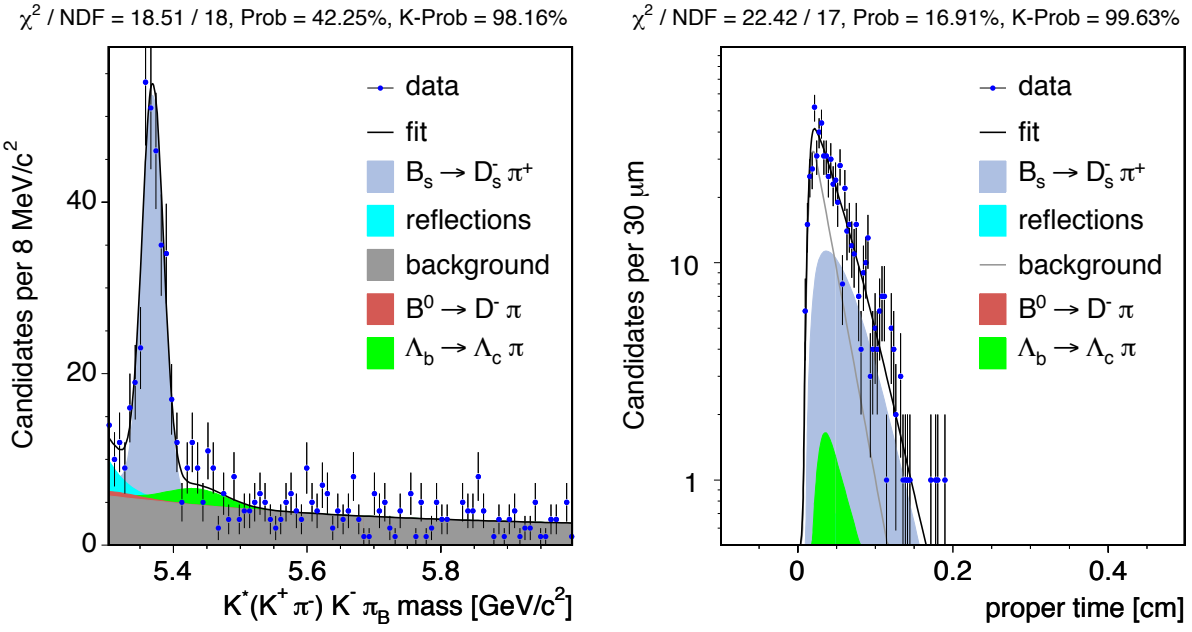

Figure 5.18: Mass and proper decay time fit projections for $B_s \to D_s^- \pi^+$ with $D_s^- \to K^{*0} K^-$.

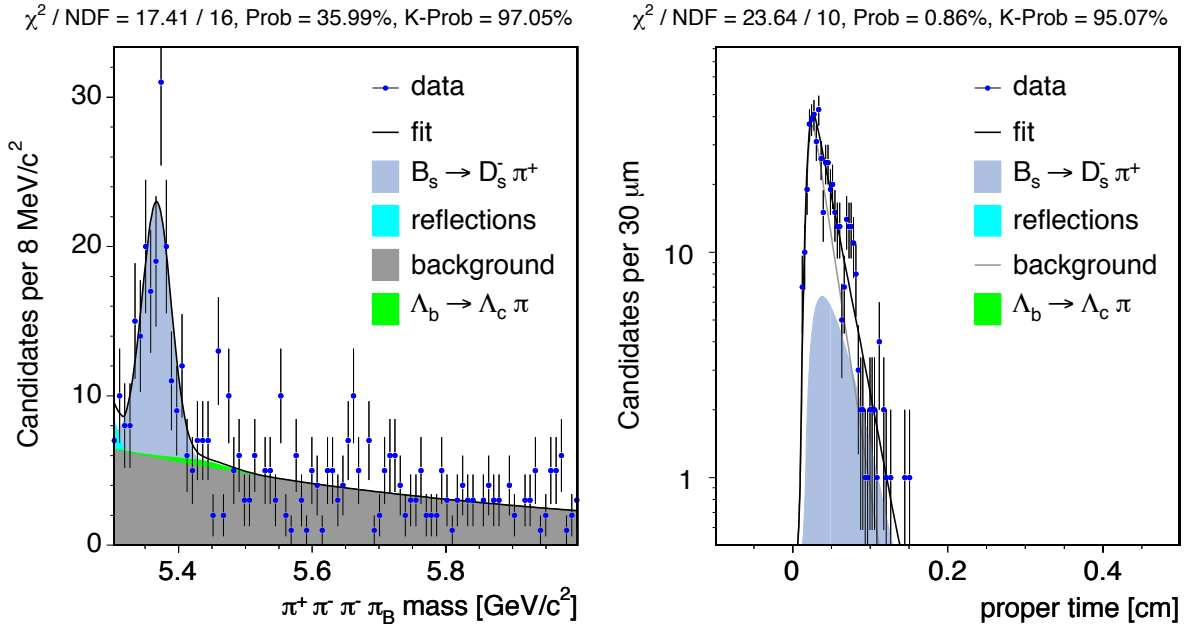

Figure 5.19: Mass and proper decay time fit projections for $B_s \to D_s^- \pi^+$ with $D_s^- \to \pi^- \pi^+ \pi^-$.

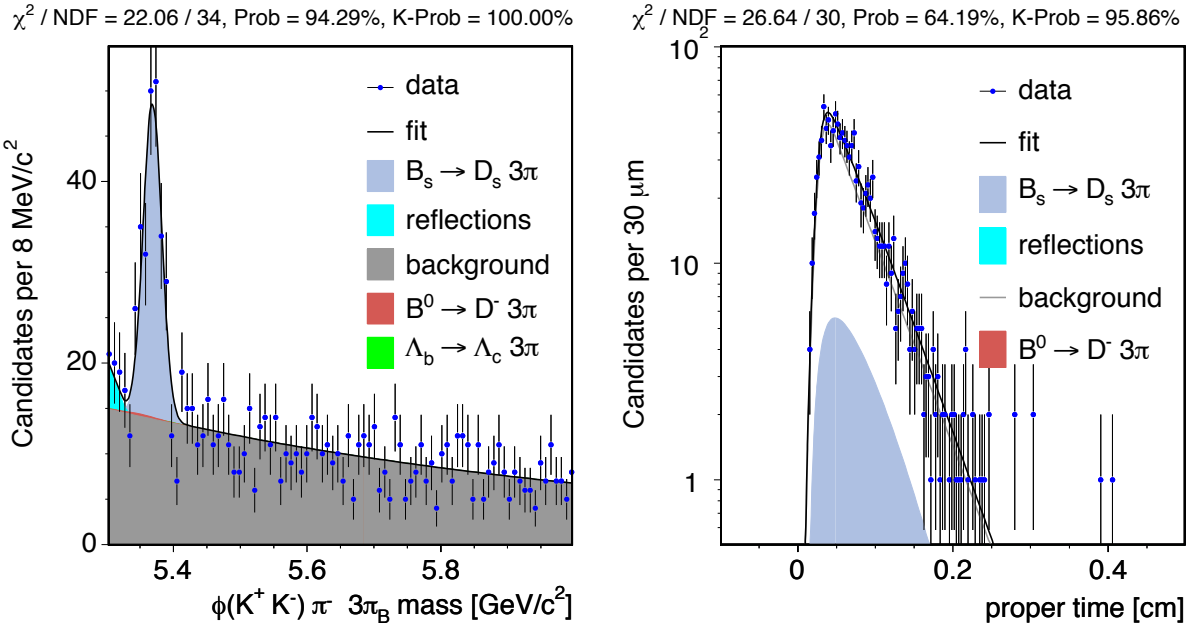

Figure 5.20: Mass and proper decay time fit projections for $B_s \to D_s^- \pi^+ \pi^- \pi^+$ with $D_s^- \to \phi \pi^-$.

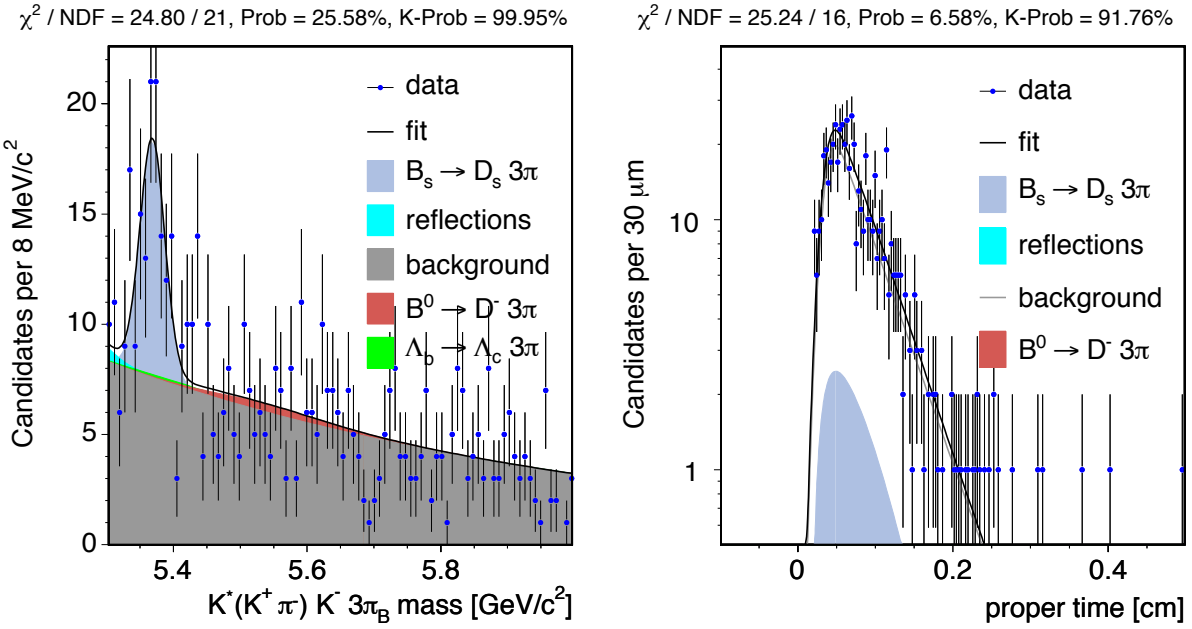

Figure 5.21: Mass and proper decay time fit projections for $B_s \to D_s^- \pi^+ \pi^- \pi^+$ with $D_s^- \to K^{*0} K^-$.

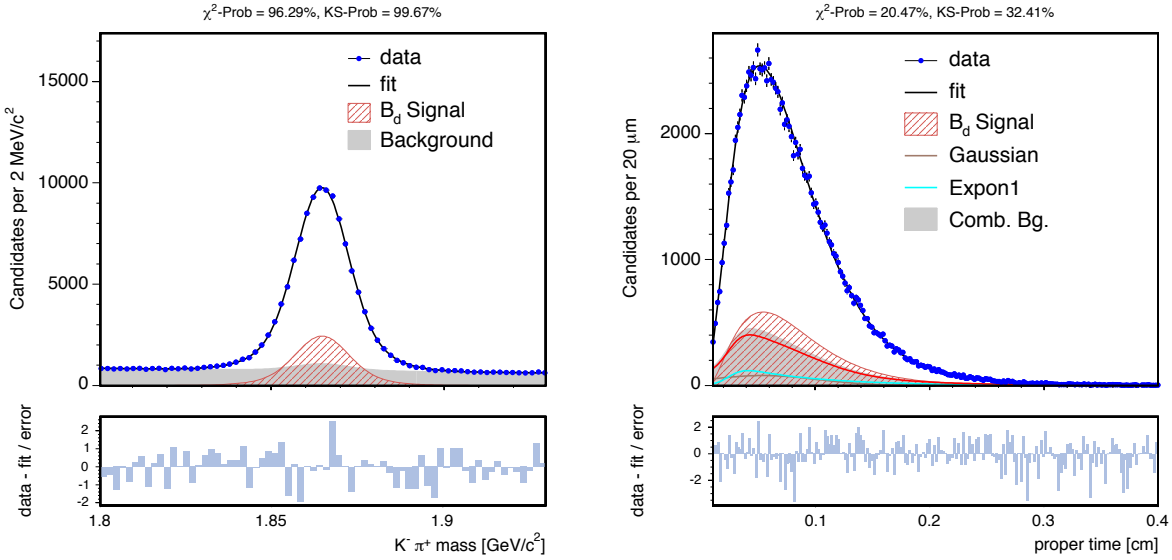

Figure 5.22: Mass and proper decay time fit projections for μD^0 B trigger.

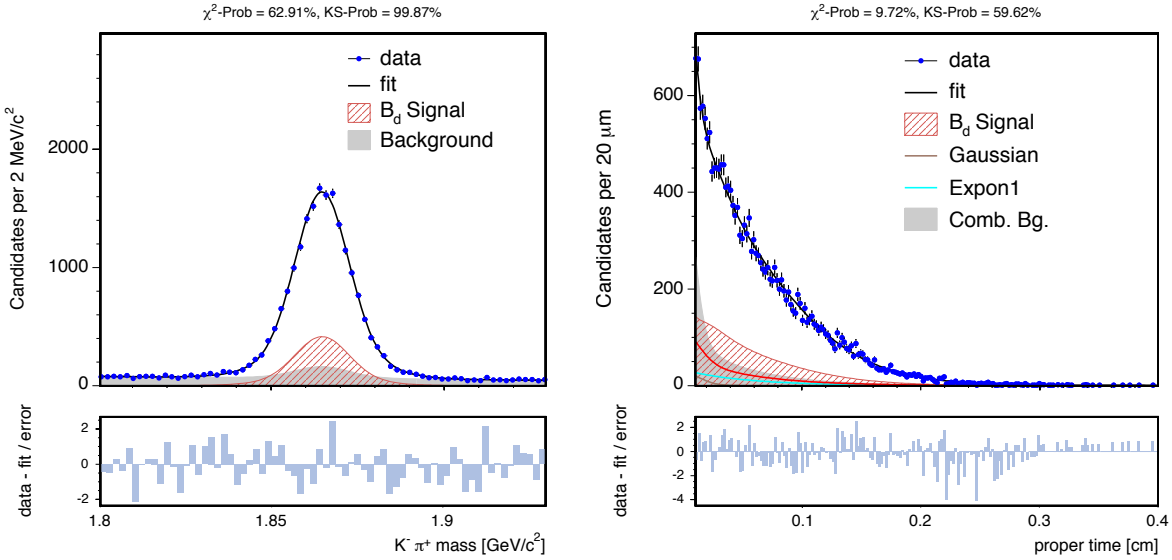

Figure 5.23: Mass and proper decay time fit projections for μD^0 D trigger.

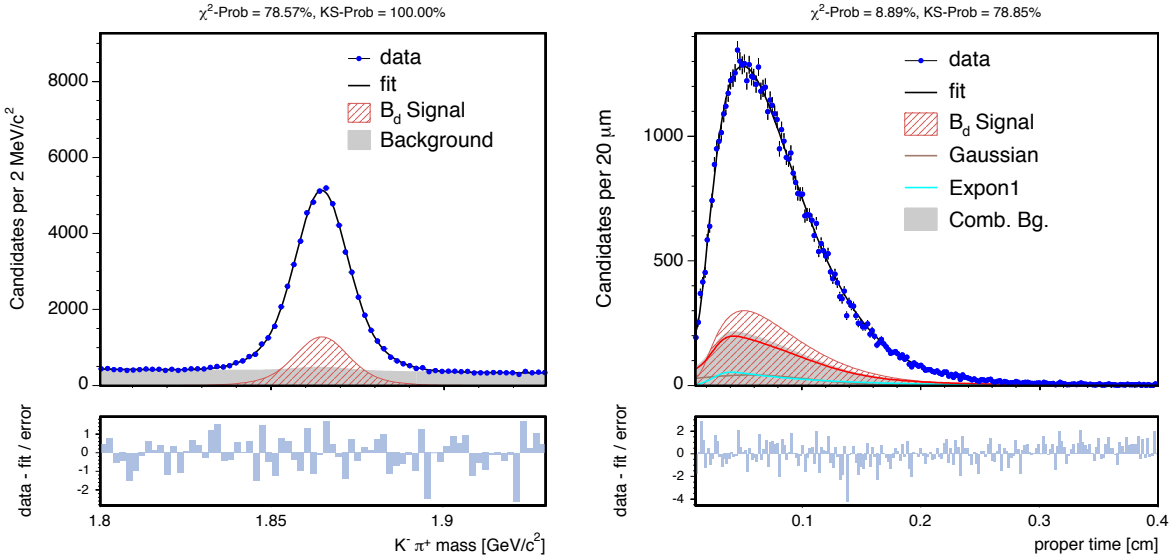

Figure 5.24: Mass and proper decay time fit projections for eD^0 B trigger.

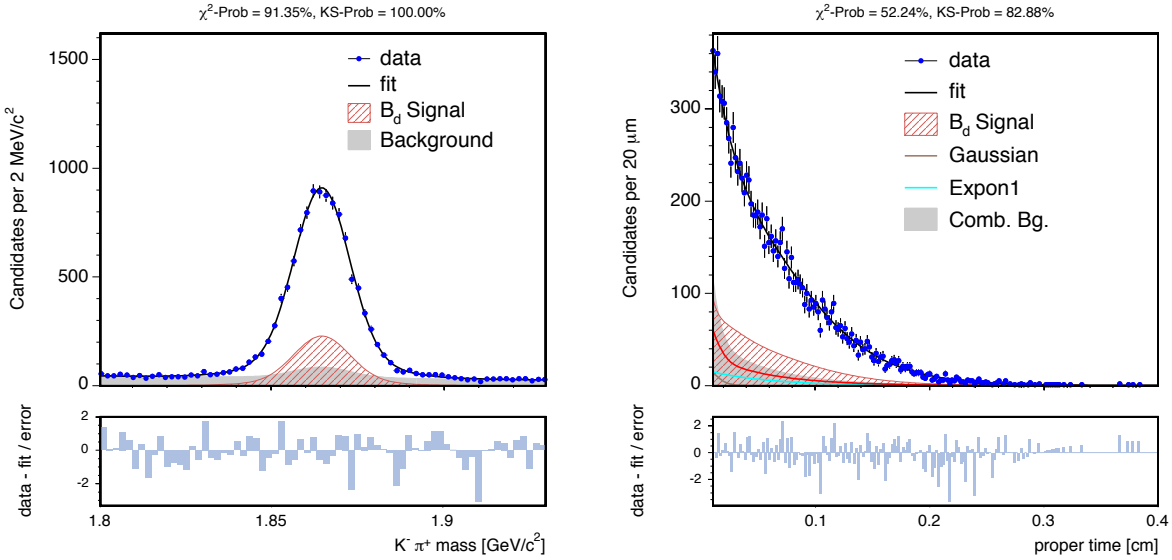

Figure 5.25: Mass and proper decay time fit projections for eD^0 D trigger.

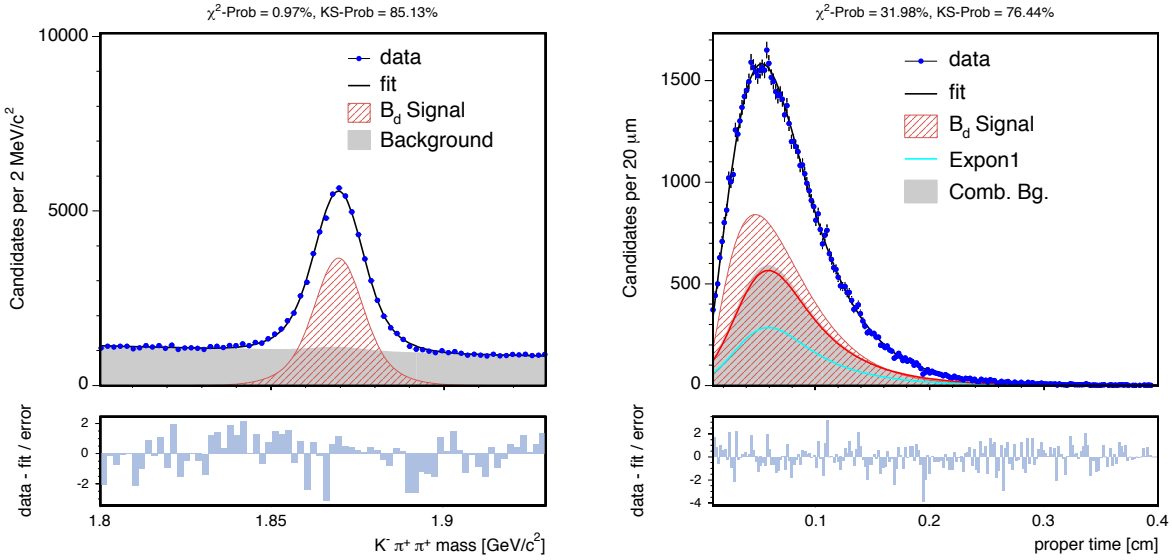

Figure 5.26: Mass and proper decay time fit projections for μD^+ B trigger.

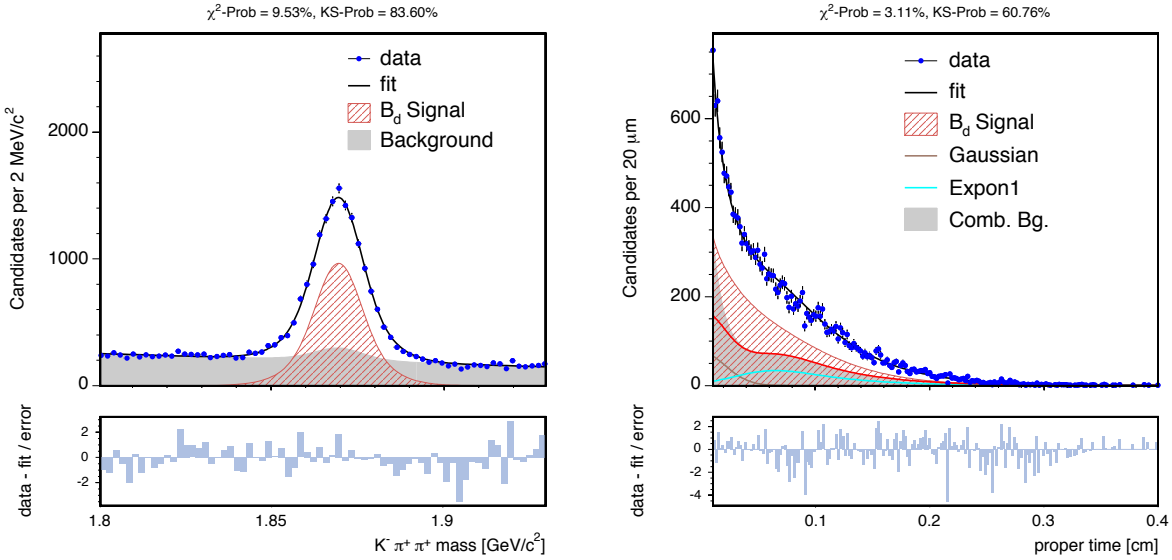

Figure 5.27: Mass and proper decay time fit projections for μD^+ D trigger.

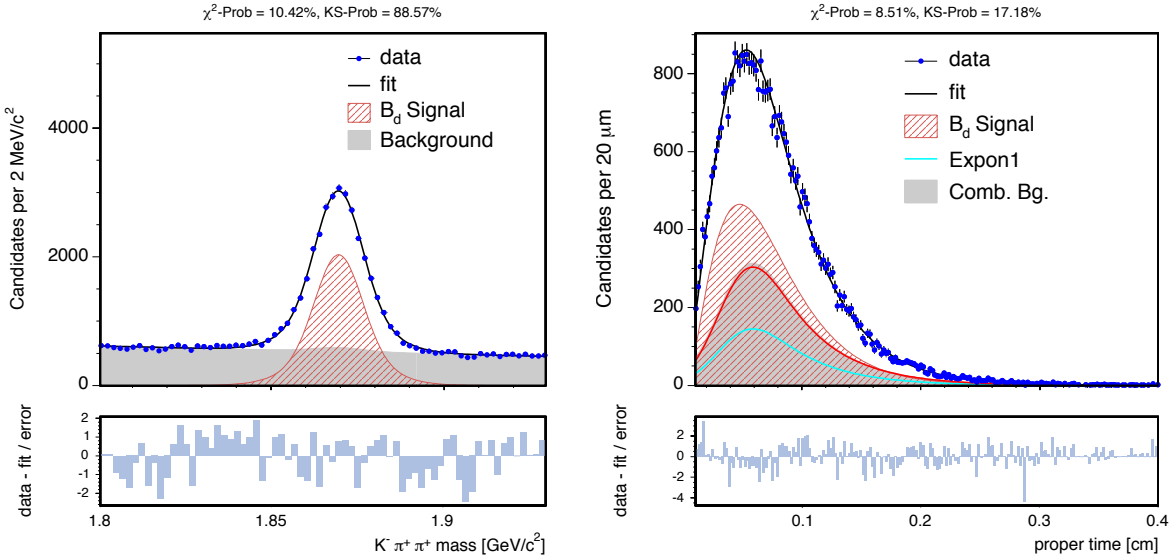

Figure 5.28: Mass and proper decay time fit projections for eD^+ B trigger.

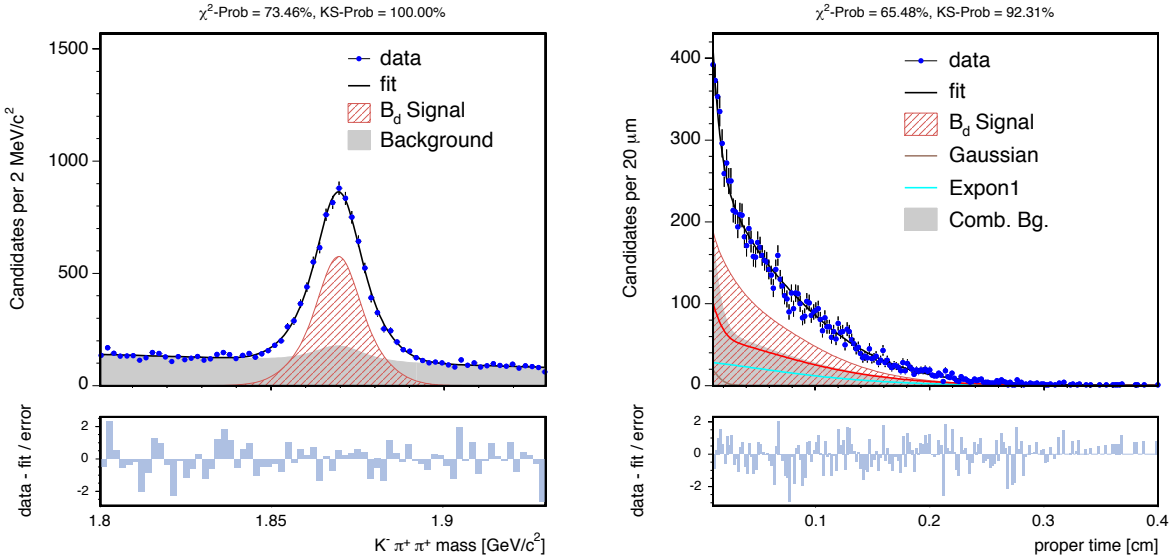

Figure 5.29: Mass and proper decay time fit projections for eD^+ D trigger.

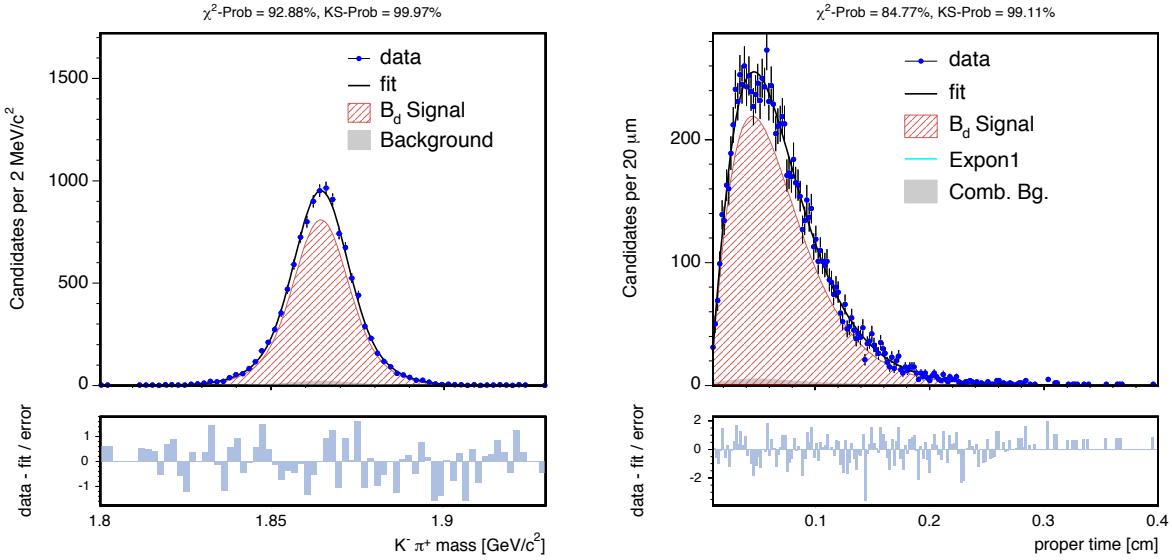

Figure 5.30: Mass and proper decay time fit projections for μD^* B trigger.

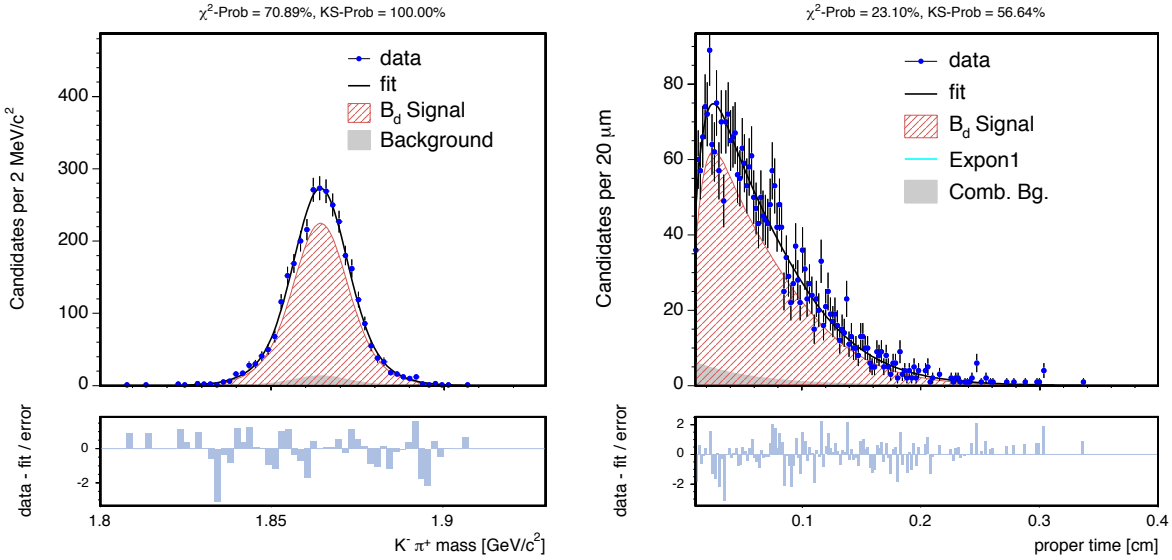

Figure 5.31: Mass and proper decay time fit projections for μD^* D trigger.

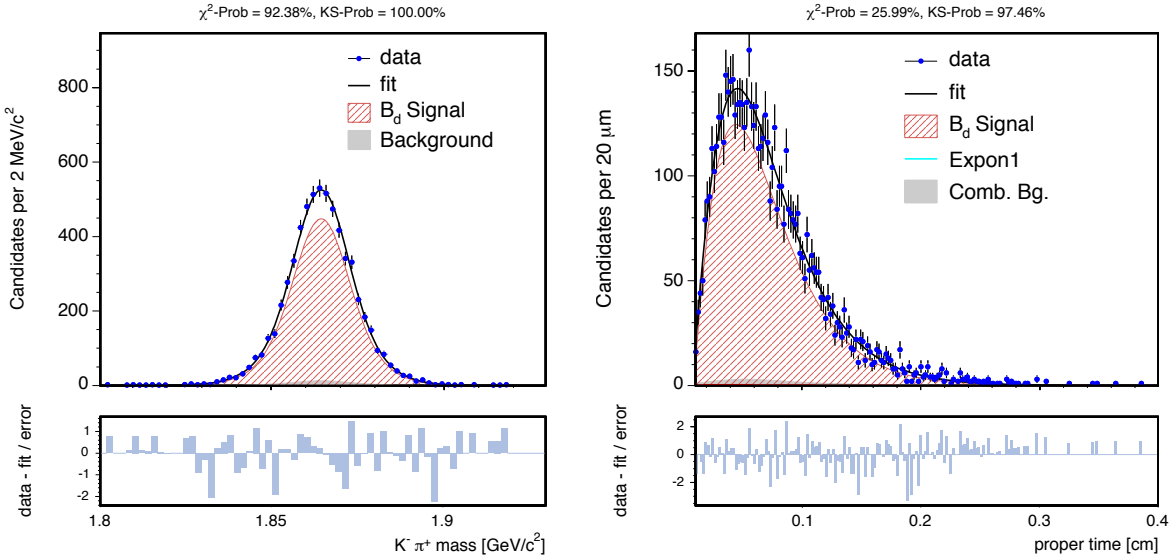

Figure 5.32: Mass and proper decay time fit projections for eD^* B trigger.

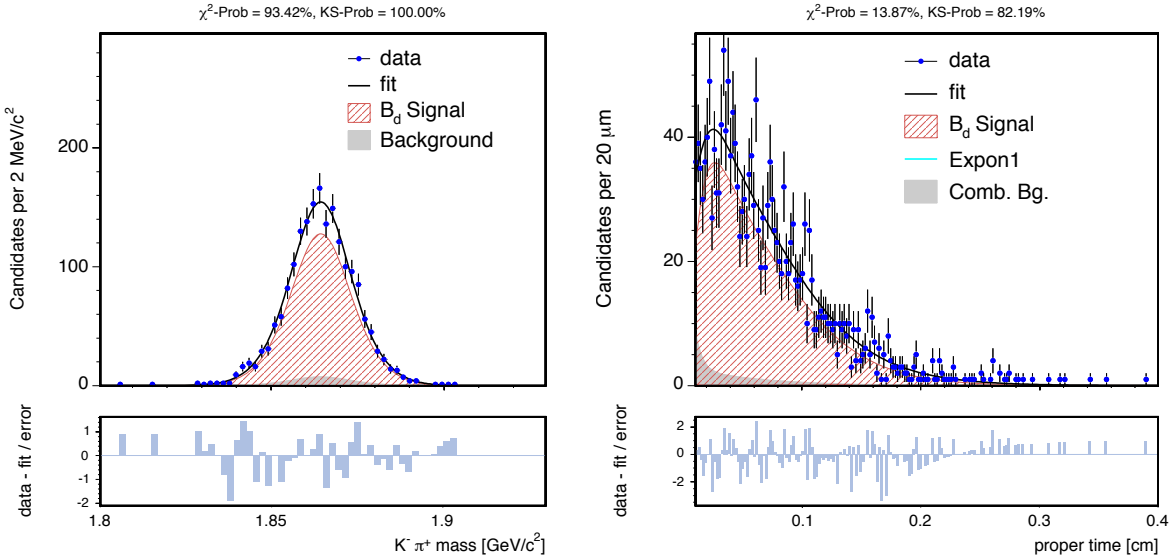

Figure 5.33: Mass and proper decay time fit projections for eD^* D trigger.

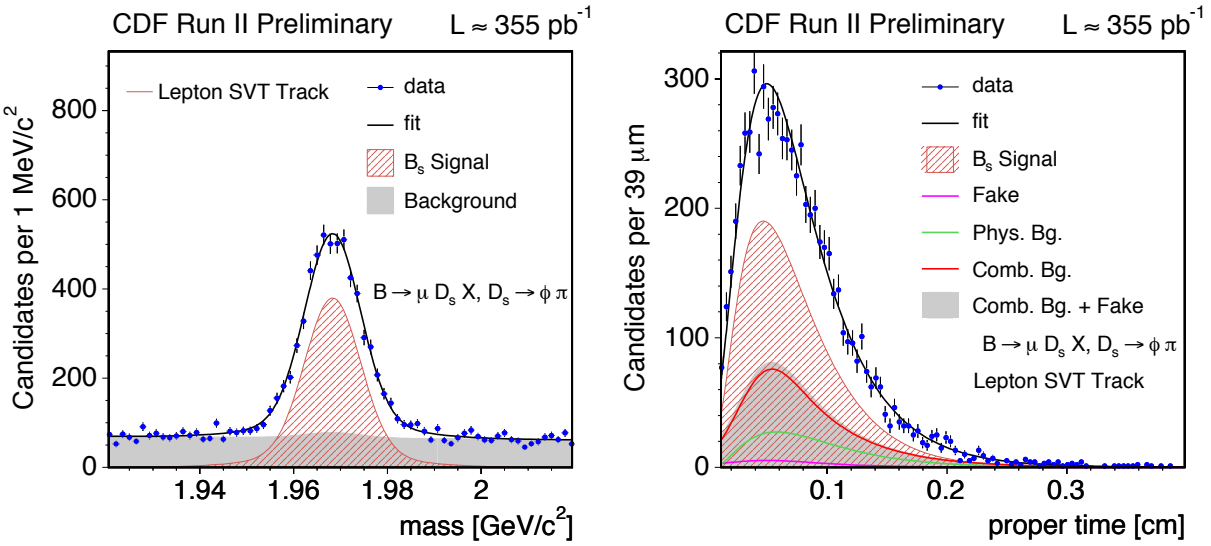

Figure 5.34: Mass and proper decay time fit projections for $\mu^+ D_s^-$ B trigger with $D_s^- \to \phi\pi^-$.

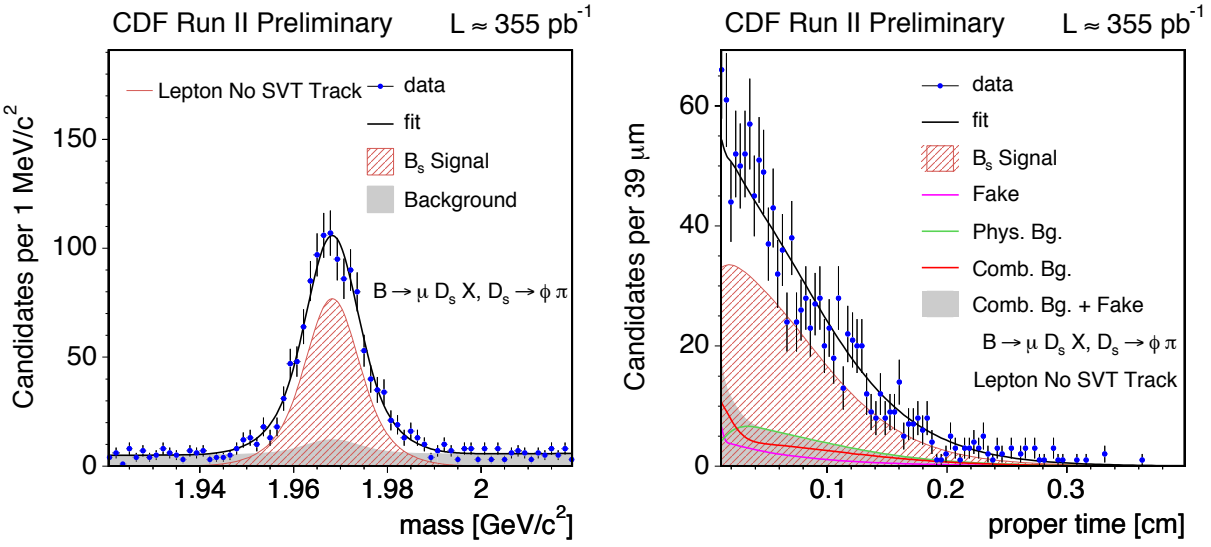

Figure 5.35: Mass and proper decay time fit projections for $\mu^+ D_s^-$ D trigger with $D_s^- \to \phi\pi^-$.

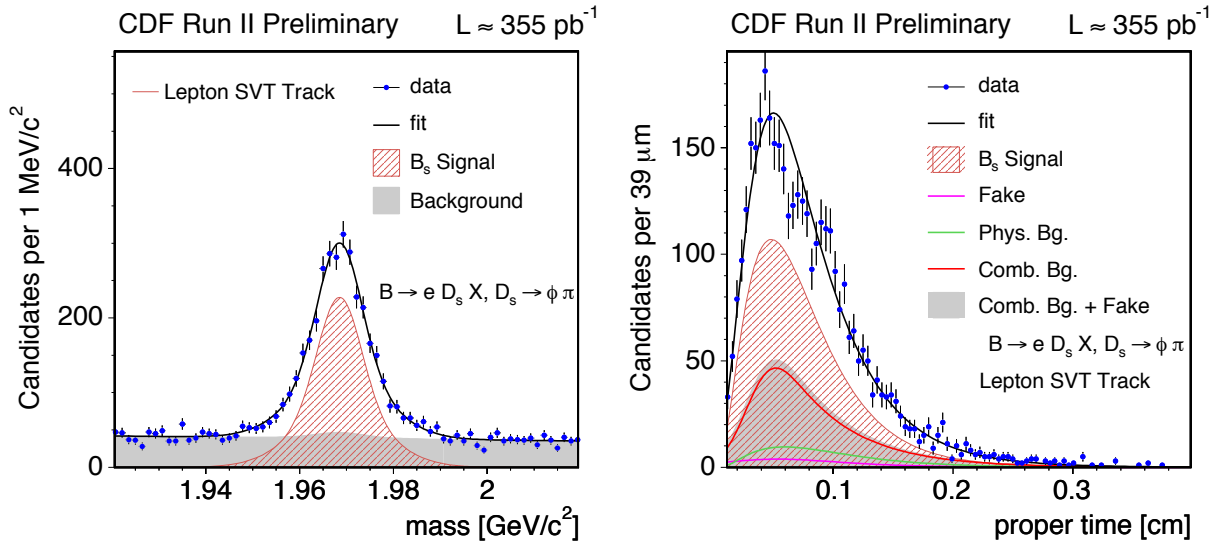

Figure 5.36: Mass and proper decay time fit projections for $e^+D_s^-$ B trigger with $D_s^- \to \phi\pi^-$.

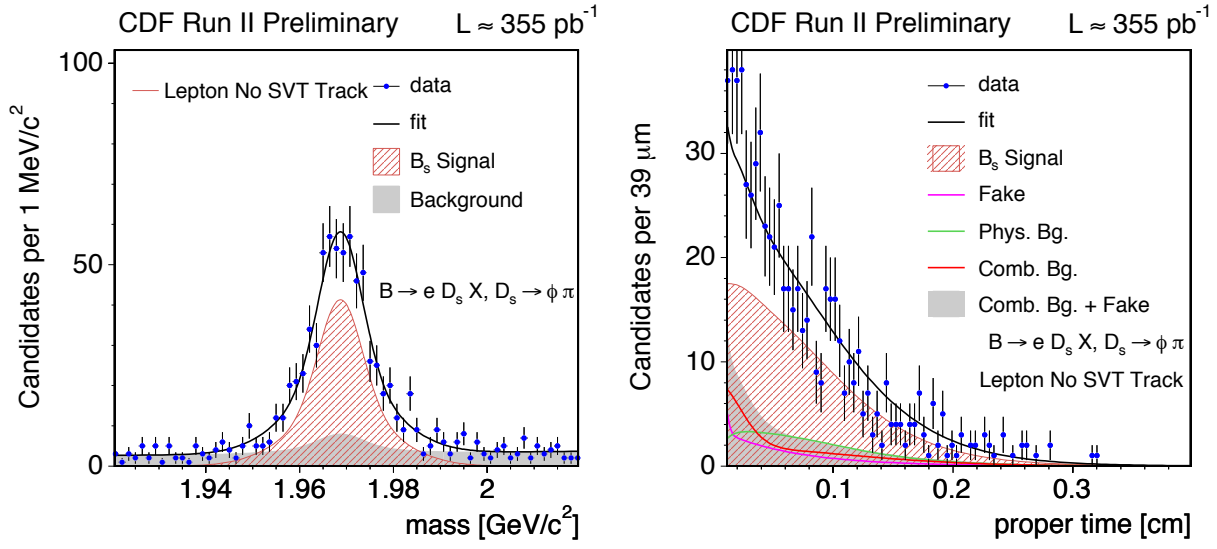

Figure 5.37: Mass and proper decay time fit projections for $e^+D_s^-$ D trigger with $D_s^- \to \phi\pi^-$.

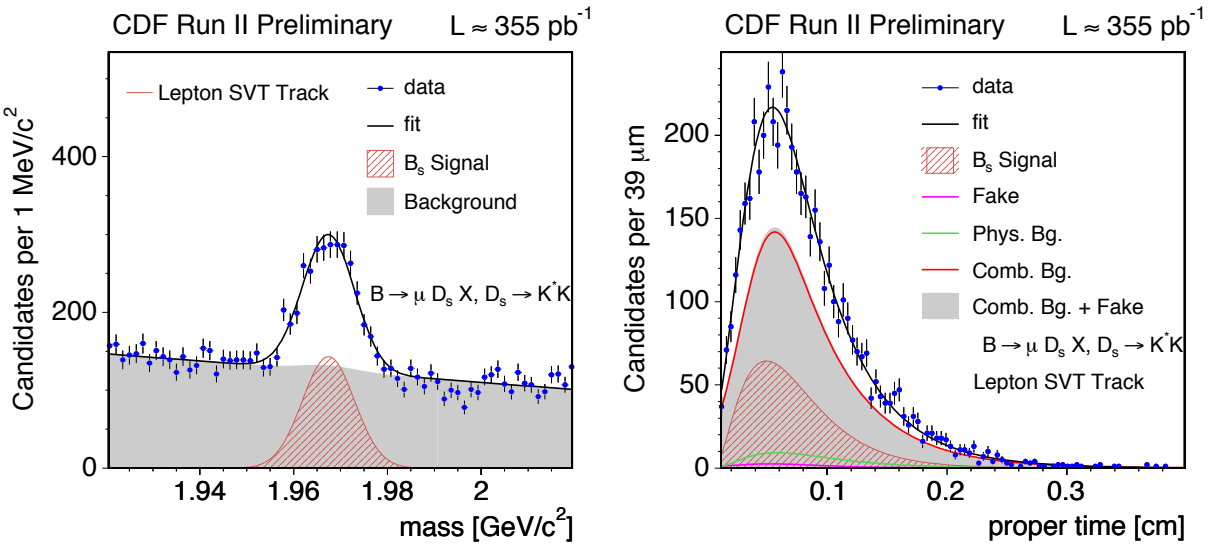

Figure 5.38: Mass and proper decay time fit projections for $\mu^+ D_s^-$ B trigger with $D_s^- \to K^{*0} K^-$.

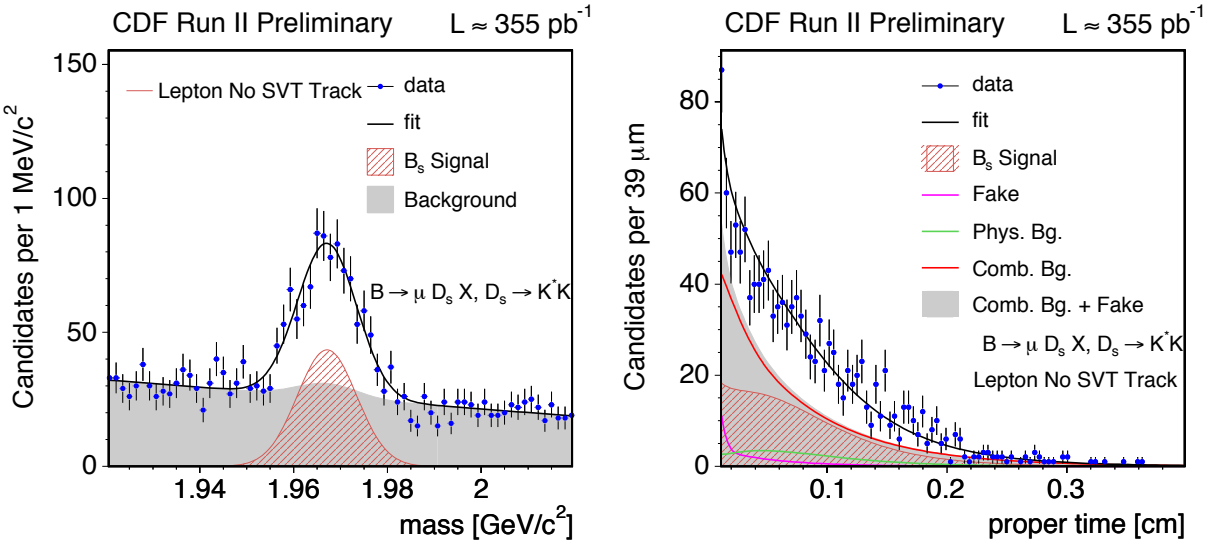

Figure 5.39: Mass and proper decay time fit projections for $\mu^+ D_s^-$ D trigger with $D_s^- \to K^{*0} K^-$.

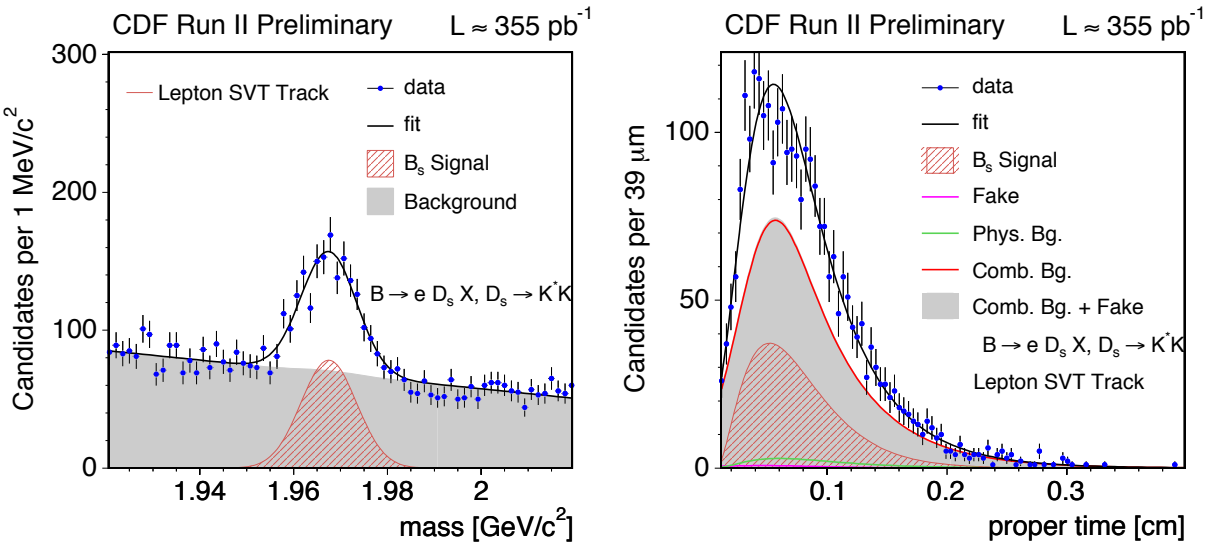

Figure 5.40: Mass and proper decay time fit projections for $e^+D_s^-$ B trigger with $D_s^- \to K^{*0}K^-$.

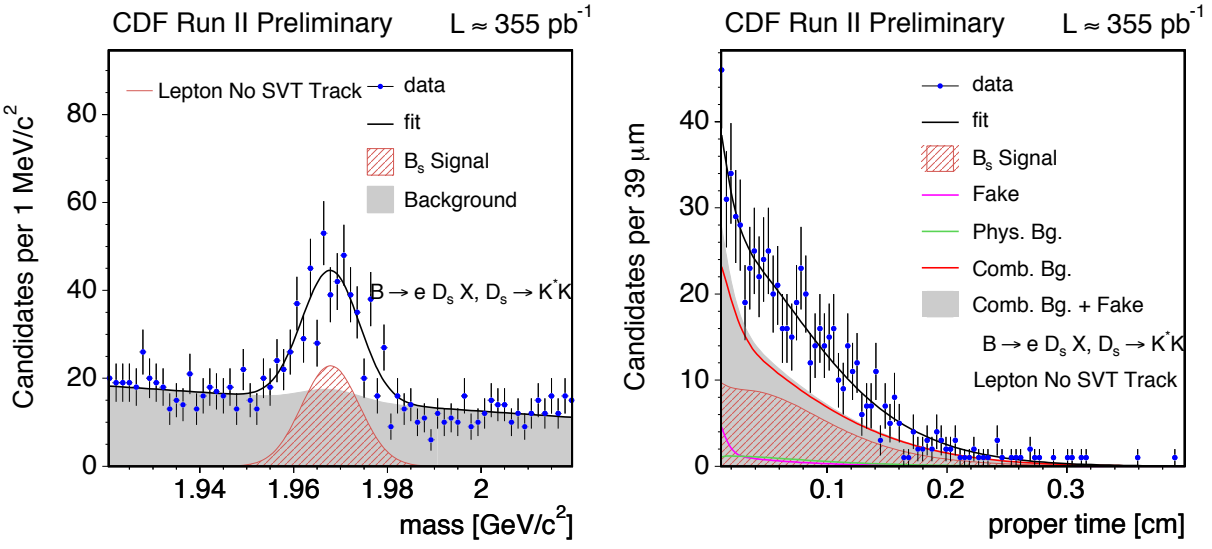

Figure 5.41: Mass and proper decay time fit projections for $e^+D_s^-$ D trigger with $D_s^- \to K^{*0}K^-$.

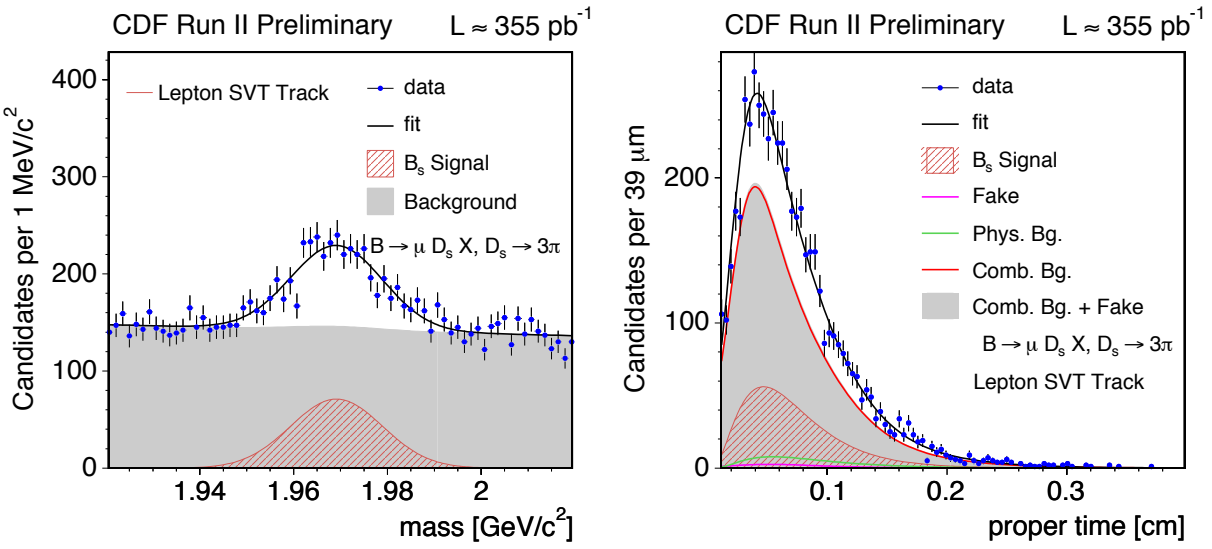

Figure 5.42: Mass and proper decay time fit projections for $\mu^+ D_s^-$ B trigger with $D_s^- \to \pi^+\pi^-\pi^-$.

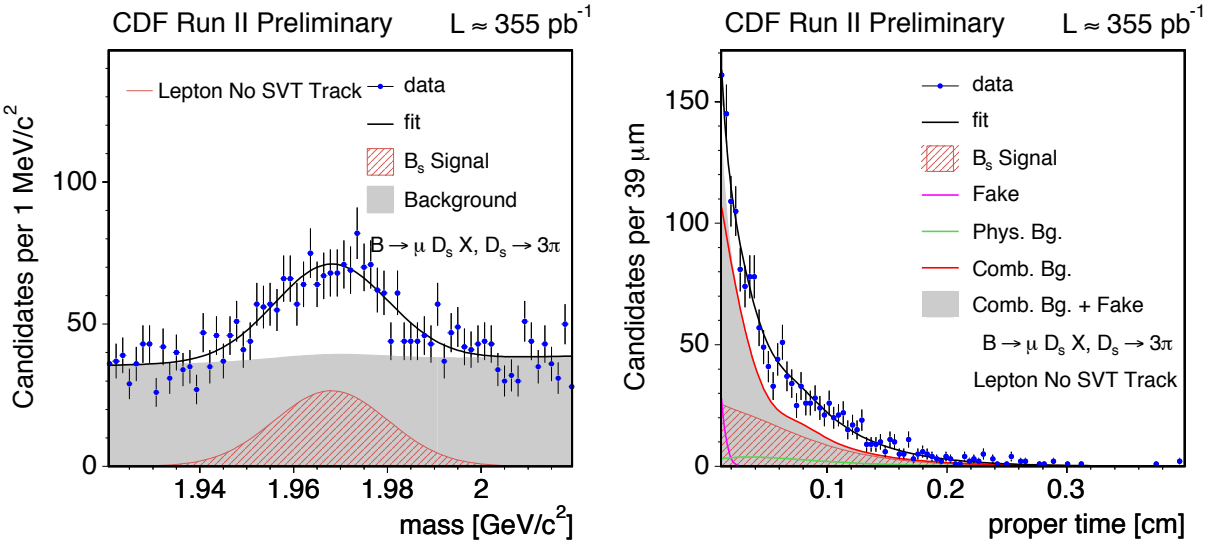

Figure 5.43: Mass and proper decay time fit projections for $\mu^+ D_s^-$ D trigger with $D_s^- \to \pi^+\pi^-\pi^-$.

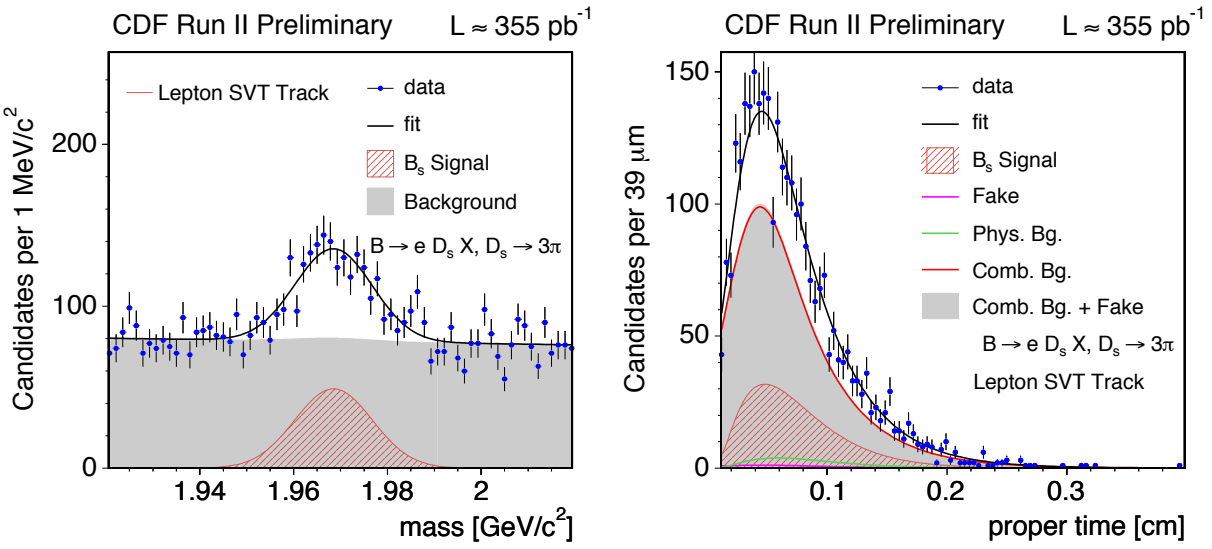

Figure 5.44: Mass and proper decay time fit projections for $e^+D_s^-$ B trigger with $D_s^- \to \pi^+\pi^-\pi^-$.

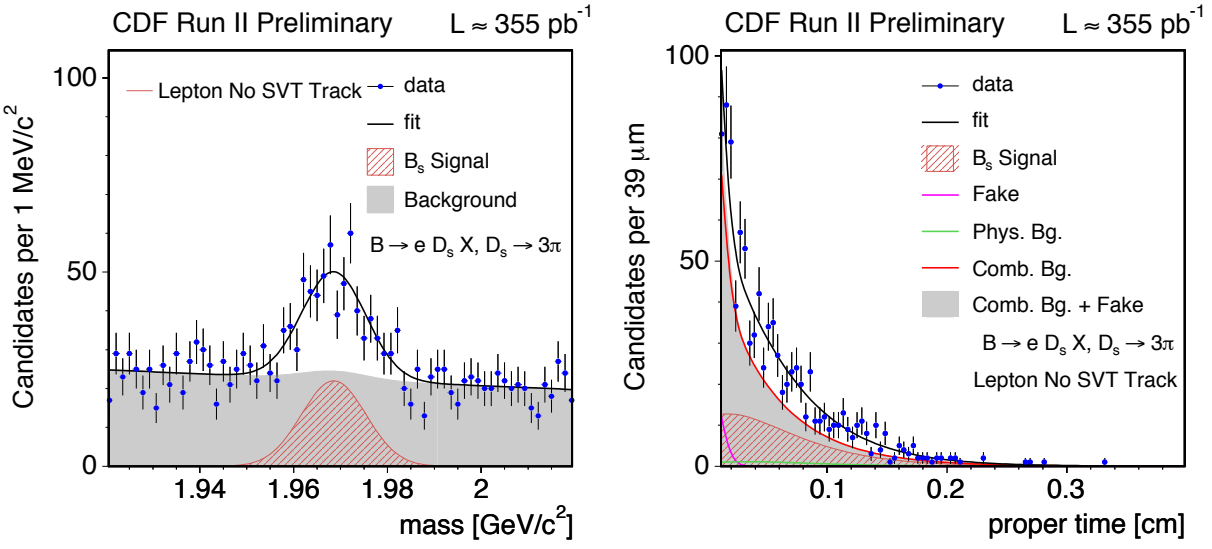

Figure 5.45: Mass and proper decay time fit projections for $e^+D_s^-$ D trigger with $D_s^- \to \pi^+\pi^-\pi^-$.

5.7 Calibration of proper time resolution

The accurate estimation of the t resolution is relevant for ensuring a precise description of the signal proper decay time distribution. It directly enters the signal PDFs. This effect becomes more conspicuously mattering in the study of t-dependent oscillations, in particular when probing high oscillation frequencies and for establishing reliable exclusion regions.

Corrections to the proper decay time uncertainty are parameterized through a *scale factor* S_t as introduced in Section 5.1.2. This factor is extracted from the data directly, namely by adjusting the width of a prompt Gaussian component describing the t distribution of combinatorial background events. This was in effect the procedure employed for the $J/\psi K$ samples where the parameter S_t is part of the fitting procedure, as expressed in (5.33), being determined predominantly from the mass-sidebands which contain a large fraction of prompt events. For the other samples, however, which are affected by the SVT trigger requirements, such prompt component is greatly reduced, and the σ_t scale factor cannot thus be determined concurrently with the fit in the exact same fashion described for the t-unbiased samples.

An alternative, more detailed approach is put forth for estimating corrections to the proper time uncertainties for the t-biased samples. It is based on a calibration sample designed to be predominantly prompt in decay time and also sharing topological and kinematic attributes with those B decay signal samples. With such a sample at hand, the same fitting framework and techniques which were described earlier in this chapter are applied to extract the scale factor values from the fit to the prompt peak. The additional background components of the sample are also described in the fit.

As already mentioned, the effect of these corrections is more determining for the study of B_s oscillations. To further facilitate the transfer of the scale factor from the calibration sample to the B_s samples its dependence on various topological and kinematical quantities is parameterized. For the B_s case therefore per-event corrections are derived based on those parameterizations. For simplicity, for the t-biased B^+ and B^0 samples a common value is derived. The proper time uncertainties σ_t, which are part of the fit input, are then re-scaled as described in (5.10) before the data is passed on to the fitter.

Calibration sample

The main intended characteristic of the calibration sample is that it be *prompt* – that is, it should contain B-like vertex candidates which are expected to coincide with the primary vertex of the $p\bar{p}$ interaction. This is accomplished by removing any requirements on impact parameter or transverse decay length which would bias or sculpt the distribution in proper decay time. Additionally, it should mimic as closely as possible the kinematics and vertex

topology of the t-biased signal samples – $B \to D\pi(\pi\pi)$ and $B \to DlX$.

The same two displaced tracks trigger dataset, from which the signal samples are extracted, is used. The method of reconstruction for the vertex candidates is to pair a real D meson with a prompt track (or three prompt tracks, depending on the channel topology) at the primary vertex. Both trigger tracks are required to be from the D meson and *not* the prompt track(s) with which it is paired. Cuts similar to those used for selecting the B samples are used, in order to have similar sample kinematics from the start. Tight cuts are also imposed on the D candidates to further maximize their signal content. Selection requirements are compiled in Table 5.11.

		$D\pi$	$D\pi\pi\pi$
$\chi^2_{r\phi}(D\pi(\pi\pi))$	$<$	15	15
$\lvert m_D - M_D\rvert$ [MeV/c^2]	$<$	8	8
$m_{D\pi(\pi\pi)}$ [GeV/c^2]		$[5.4, 6.0]$	$[5.4, 5.8]$
$m_{\pi\pi\pi}$ [GeV/c^2]	$<$	—	1.75
$p_T(D\pi(\pi\pi))$ [GeV/c]	$>$	5.5	6.0
$p_T(\pi)$ [GeV/c]	$>$	1.2	—
$\lvert d_0(D)\rvert$ [μm]	$<$	100	100

Table 5.11: Selection requirements for σ_t calibration sample.

The resulting calibration sample is larger than the corresponding hadronic B_s samples by a factor of ~ 500 for the $D\pi$ topology and ~ 100 for the $D\pi\pi\pi$ topology.

Global fit

A fit is performed to the proper decay time distribution of the sample. No distinguishing structures exist in mass space between the components of the sample, and the likelihood is given by the t-PDF only. The latter corresponds to a model similar to that used for parameterizing the combinatorial background in t-unbiased samples given by (5.33). The dominant component is, as designed, given by a prompt Gaussian. It is formed of events containing a real, prompt D meson and one (three) prompt track(s). In addition, there is a smaller contribution [75] from secondary D mesons originating from B decays, misreconstructed D mesons, and tracks not originating from the primary vertex. These are described by negatively and positively lived exponential tails of the form of (5.31). More specifically, and in addition to the prompt component, the $D\pi$ topologies are found to be best fitted with one long lived and one short lived exponential tail pair symmetric about zero,

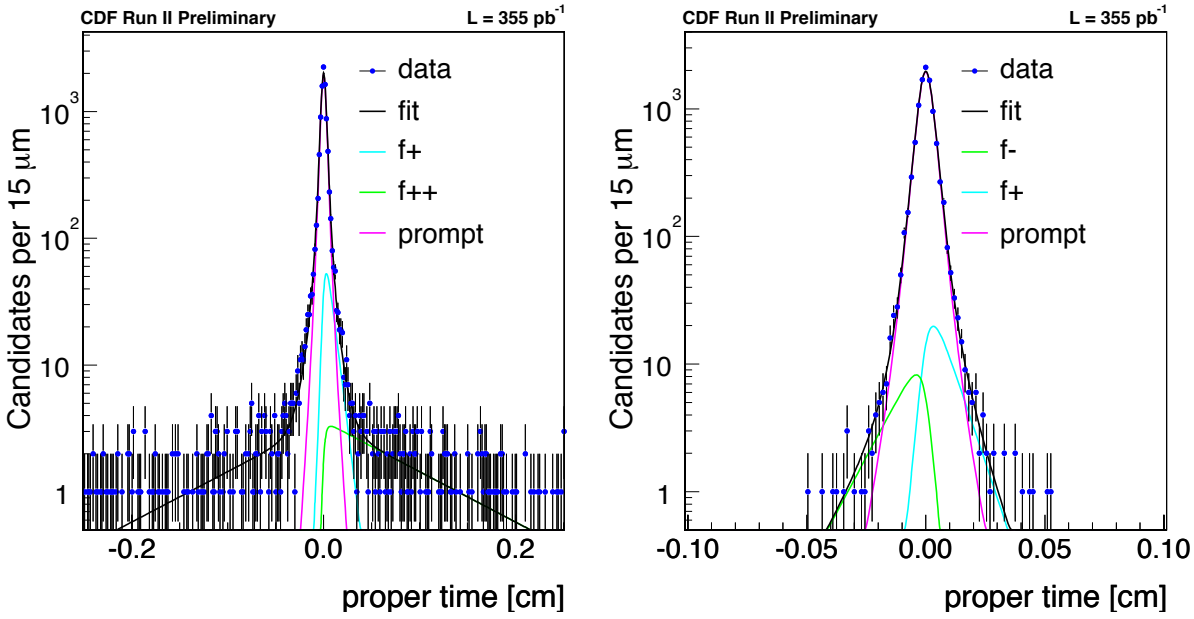

Figure 5.46: Representative t distributions and fit projections for the $D\pi$ (left) and $D\pi\pi\pi$ (right) topologies.

while for the $D\pi\pi\pi$ topologies a single asymmetric exponential tail pair is found to form an adequate model. Representative t distributions and associated fit projections for the $D\pi$ and $D\pi\pi\pi$ topologies are shown in Figure 5.46.

The components just described which make up the PDF correspond to a delta function (5.30) and exponential (5.31) functions, convoluted with a Gaussian resolution function, $G(t; S_t\sigma_t)$, whose width is given by the candidate's measured t uncertainty multiplied by the scale factor, S_t. The latter, which is common to all PDF terms, is the fit parameter of interest. Table 5.12 lists the scale factor fit results for the total sample. These corroborate the value of 1.4 which was chosen as the common scale factor value to be used for all B^+ and B^0 t-biased samples.

topology	N	S_t
$D\pi$	338000	1.406 ± 0.003
$D\pi\pi\pi$	35500	1.492 ± 0.008

Table 5.12: Total sample size N and fitted scale factor S_t for the calibration sample topologies; uncertainties are statistical only.

Scale factor dependencies and tuning

We now pursue a parameterization of the scale factor based on a set of variables on which it is observed to have dependence. These dependences are then used to estimate the scale factors for the signal samples on a per-event basis. The motivation for doing so is two-fold. It allows for a more systematic and proper transfer between the calibration and the signal samples, by effectively taking into account relative *kinematical* differences. Additionally, by scaling the measured proper time resolution by different values, candidates with good resolution are identified and used to the fullest extent, while candidates with poorer resolution are de-weighted in the smearing (5.14) of the signal PDF.

Due to its large size, the calibration sample can be binned in different variables and examined for the dependences of S_t. The following set of variables characterizing the $D\pi(\pi\pi)$ system is employed in the parameterization:

- angular distance (between the D and the pion(s)), ΔR,
- isolation, $I = p_T(D\pi(\pi\pi))/\sum_i p_T^i(\Delta R < 0.7)$,
- pseudo rapidity, η,
- beamline axis position, z,
- chi-square of the vertex fit in the transverse plane, χ^2.

Figure 5.47 overlays the distributions of the calibration sample and the sideband-subtracted signal samples $B_s \to D\pi/l$, for the selected variables. The disagreements in these distributions are not of concern, precisely because the respective dependences of S_t are parameterized (Figure 5.48). Rather, the important consideration here is that the calibration sample covers the phase space of the signal samples.

The scale factor parameterization is implemented by factorizing the dependence on the various variables, that is

$$S_t(\Delta R, I, \eta, z, \chi^2) = f_{\Delta R} \cdot f_I \cdot f_\eta \cdot f_z \cdot f_{\chi^2} \ , \tag{5.36}$$

where the various f denote polynomial functions (in fact, parabolas) obtained by fitting the dependence on the individual quantities as illustrated in Figure 5.48. The polynomial parameters are adjusted in an iterative fashion. That is, the scale factor variation with respect to one quantity is first fitted and corrected for, and then the correction for a succeeding variable is extracted and applied. The pattern is continued until the parameterized scale factor produces a reasonably constant behavior close to unit. This is illustrated in Figure 5.48 where

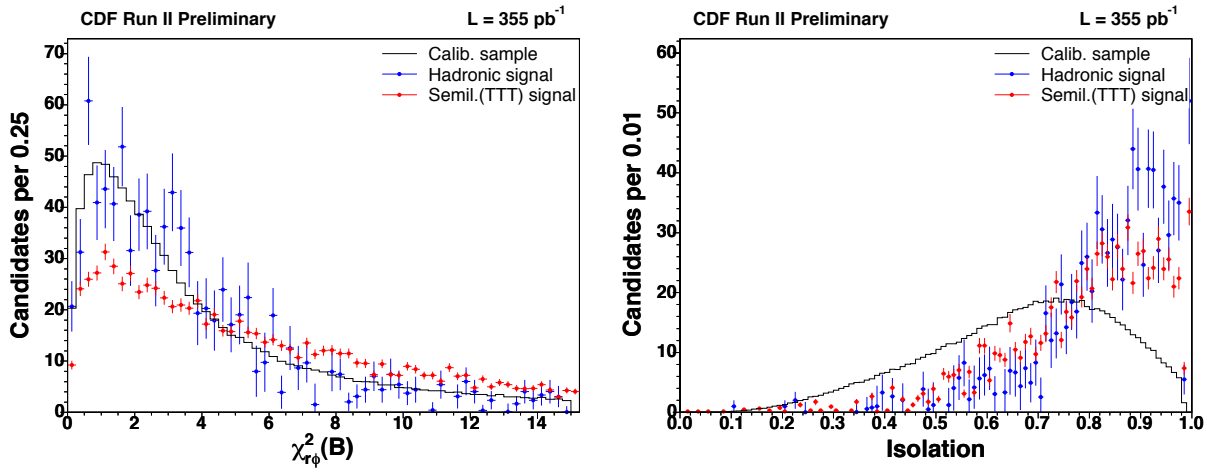

Figure 5.47: Comparison of the calibration sample (black line) and sideband-subtracted $B_s \to D_s\pi/l$ distributions of variables from hadronic (blue) and semileptonic (red) samples, for the variables $\chi^2(B)$ (left) and isolation (right). Distributions are scaled to facilitate comparison.

the original dependence patent on the leftmost plot is absorbed once the parameterization is applied as it is seen in the rightmost plot.

It is the tuned parameterization achieved in (5.36) that is used to scale the proper time uncertainties (5.10), according to the individual candidates' characteristics, in the case of the B_s signal samples. In Table 5.13 we summarize the average of the corrections to σ_t implemented in the various hadronic B_s modes.

$B_s \to D_s^-\pi^+$, $D_s \to \phi\pi$	1.44137
$B_s \to D_s^-\pi^+$, $D_s \to K^*K$	1.39889
$B_s \to D_s^-\pi^+$, $D_s \to \pi\pi\pi$	1.37909
$B_s \to D_s^-\pi^+\pi^-\pi^+$, $D_s \to \phi\pi$	1.39659
$B_s \to D_s^-\pi^+\pi^-\pi^+$, $D_s \to K^*K$	1.39722

Table 5.13: Average correction factors to σ_{ct} for different B_s modes.

Systematic uncertainties

Systematic aspects associated to the method employed for deriving the corrections to the proper time uncertainties are now addressed. Foremost, we intend to ensure that the achieved

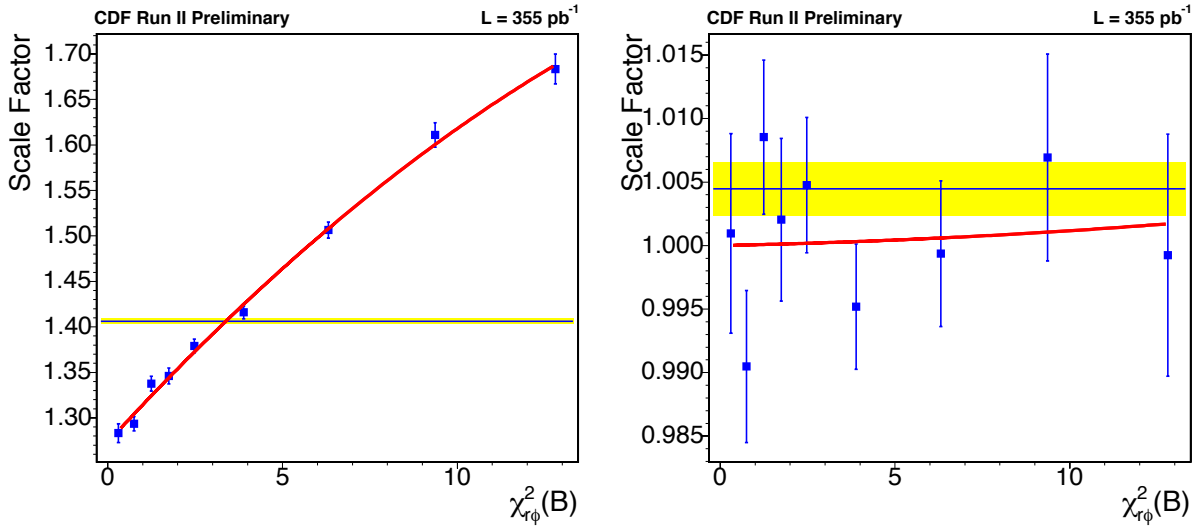

Figure 5.48: Scale factor dependence before (left) and after (right) parameterization, illustrated for the χ^2 vertex fit in the $D\pi$ topology.

corrections are not incorrectly favorable when establishing exclusion conditions for the oscillation frequency. Hence only an upper bound on the scale factor is measured.

The following systematic sources are considered.

***D* background content:** The likelihood model used for fitting the calibration sample employs several simplifications. A main assumption in this respect is that the D candidates are purely signal, in view of the tight D selection requirements, and no modeling of combinatorial D background is thus included. To evaluate the effect of this model simplification we increase, by approximately two times, the level of background acceptance in the sample by doubling the width of the D mass cut window. We then determine the shift in the fitted average scale factor values on this background-enriched sample.

***D* impact parameter requirement:** The requirement on the D impact parameter is used to select candidates whose momentum points to the primary vertex. This may bias the vertex calibration by preferentially rejecting badly measured events which could have large scale factors. To evaluate this effect the impact parameter selection requirement is varied by 20 μm around the nominal 100 μm cut, and the modified samples are fitted for the average residual scale factors.

Transferred parameterization: The scale factor parameterization is to be applied to the various B_s signal modes. While it is derived in a calibration sample involving only D^- candidates, those target B_s samples are based on distinct D_s topologies. Other calibration topologies were designed, including $D_s\pi$, $D^0\pi$, and additional $D\pi\pi\pi$ modes. The systematic

uncertainty associated with the transfer of scale factors between different D decay topologies is evaluated by fitting for the average scale factors in the various samples with interchanged parameterizations; the largest observed deviation from unit is taken as the uncertainty.

Tuning residuals: The tuning procedure employs a limited number of variables while there may be others on which the scale factor also depends. The assumption was also made that the dependences completely factorize. The effect of such incompleteness of the tuning procedure is small and limited to the level of the residual deviations from the average fitted scale factor. These are taken as the dominant relative systematic uncertainty source. The relative systematic uncertainties evaluated for each source are shown in Table 5.14.

systematic source	relative uncertainty [%]
D background	< 1.0
D impact parameter	≤ 1.0
transferred parameterization	3.5
tuning residuals	4.0
total assigned	6.0

Table 5.14: Contributions to the σ_t scale factor systematic uncertainty.

5.8 Résumé

The unbinned fitting framework and associated likelihood description of the data samples in mass and proper decay time spaces in the absence of flavor tagging information have been presented.

The quantities of central interest for this dissertation are associated directly to the description of the proper decay time of the reconstructed B meson signals in the data samples. The discrimination of these signals from the various other components which constitute the samples chiefly benefits from the characterization of the involved mass distributions. The fits of the data are accordingly performed based on input information from both proper time and mass spaces in a concurring fashion. This input data is moreover provided for the individual B mesons candidates, thus following an unbinned approach, which maximizes the usage of the available information extracted from the data samples.

The components which contribute to the data samples were identified in Chapter 4. Each of these components is modelled in the spaces of the input quantities to the likelihood function. The characterization of background contributions of the combinatorial type is inferred from mass-sideband regions, while that of backgrounds of the physics type, originating from

non-signal b-hadron decays, readily benefits from expected templates found from Monte Carlo simulation of those processes. The B signals are recognized in mass space as Gaussian peaks whose widths are determined by the detector resolution.

The B mesons lifetimes, here the main parameters of interest, are part of the proper decay time probability density functions for signal components. Analysis methods are developed in order to give necessary account of effects coming from trigger and selection requirements, and partial reconstruction which characterize the data samples. Analytical techniques are further examined and implemented that result in an optimization of speed and accuracy of the fitting process.

The measured B meson lifetimes are summarized (uncertainties are statistical only):

	lifetime, τ [ps]
B^+	1.654±0.008
B^0	1.557±0.007
B_s	1.479±0.020

These are found to be in good agreement with the world average values [1] —1.670 ± 0.017 ps (B^+), 1.535 ± 0.014 ps (B^0), 1.460 ± 0.057 ps (B_s). The statistical precision achieved is competitive with those averages. Preliminary evaluation of the systematic uncertainties performed in previous iterations of the analysis estimate less than 4% relative systematic uncertainty contributions.

The issue of proper time uncertainty calibration, of particular relevance for the study of B_s oscillations, is also thoroughly addressed.

The fitting framework here described further provides the underlying structure for the study of neutral B meson mixing once treatment of flavor information is incorporated. This information is acquired by applying to the data samples flavor tagging techniques. Such are the matters to be explored in the ensuing chapters.